Embryonic Stem Cells and Plasmid Transfection

We used the embryonic stem (ES) cell line TT2, as described previously [12]. The ES cells (2×10^5 cells) were precultured for 24 h in gelatinized six-well dishes under a feeder-free condition, and the plasmids were transfected into ES cells using Lipofectamine 2000, in accordance with the manufacturer's instructions(Invitrogen).

Animals

NOD.CB17-*Prkdc*^{scid}/J (NOD/SCID) mice, ICR mice, and C57BL/6J mice were obtained from Charles River Japan Ltd. The animals were housed in cages (five animals per cage) and were provided access to water and food (LabDiet 5053; Purina Mills, Richmond, IN) ad libitum. The animal rooms were maintained under a temperature-controlled (21°C–25°C) and light-controlled (12L:12D cycle, lights-on at 0900 h) environment. All of the mice were bred and maintained under specific pathogen-free conditions. The methods used for animal care and the experimental procedures were approved by the Animal Care Committee of the University of Tokyo.

In Vitro Fertilization

Female mice (age 4 wk) were superovulated by i.p. injection of 5.0 IU of equine chorionic gonadotropin (Serotropin; ASKA Pharmaceutical Co. Ltd.) at 2000 h, followed by injection of 5.0 IU of human chorionic gonadotropin (Gonatropin 3000; ASKA Pharmaceutical) 48 h later. The oocytes were collected 14 h after the human chorionic gonadotropin injection, according to standard procedures [13]. The cumulus-oocyte complexes were isolated from the oviducts in a 500-μl human tubal fluid (HTF) drop under mineral oil. The cauda epididymides were dissected from 10- to 12-wk-old male mice, and the sperm were isolated in a 500-μl HTF drop under mineral oil. The sperm were activated in the HTF drop under mineral oil for 1 h. All of the oocytes were added immediately to the appropriate fertilization dishes containing the activated sperm samples. After 6 h of incubation (5% CO_2, 37°C, and 95% humidity), the oocytes were washed through a 200-μl drop of M16 medium and incubated in a CO_2 incubator in a 200-μl drop of M16 medium until the microinjection.

Pronuclear Microinjection and Transfer of the Two-Cell-Stage Embryos

Transgene DNA was injected via needles pulled from 1-mm outer diameter, 0.75-mm inner diameter glass capillaries with internal filaments (World Precision Instruments) on a Sutter P-97 micropipette puller (Sutter Instrument Co.). The P-97 was configured as follows: 4.5-mm trough filament, heat set to 730, pull set to 0, velocity set to 30, time set to 250, heat set to 730, pull set to 80, velocity set to 60, and time set to 200. The microinjection needles containing the transgene DNA were connected to the pneumatic microinjector, FemtoJet (Eppendorf Co. Ltd.). The micromanipulation workstation consisted of a Leica DM IRB Inverted Research microscope (Leica Microsystems Inc.) equipped with differential interference contrast optics and a Micromanipulator 5171 (Eppendorf). At 8 and 15 h after the IVF, fertilized eggs with visible pronuclei were selected for the microinjection, and unfertilized eggs were discarded. After the microinjection, the eggs were cultured overnight in a 200-μl drop of M16 medium up to development of the two-cell-stage embryos. The two-cell-stage embryos were transferred to the oviducts of pseudopregnant recipients, and the egg recipients were housed in cages (two to three per cage).

PCR and Southern Blot Analysis

DNA extracted from the tail tips of the weaned pups was subjected to 30 cycles of PCR amplification with primers for EGFP—forward, 5′-GACGGC GACGTAAACGGCCA-3′, and reverse, 5′-GCCCCAGGATGTTGCCGTCC-3′—to check for integration of the EGFP transgene(s). For Southern blot analysis, genomic DNA (5 μg) was digested with *Xho*I, separated by electrophoresis on a 0.6% agarose gel, and blotted onto a nylon membrane before hybridization with the 32P-random-prime-labeled, 361-bp integrated EGFP fragment amplified by PCR.

Microscopy

The transfected ES cells and the Tg mice generated as above were examined using a macrofluorescence microscopy system (VB-G05; Keyence Japan Inc.).

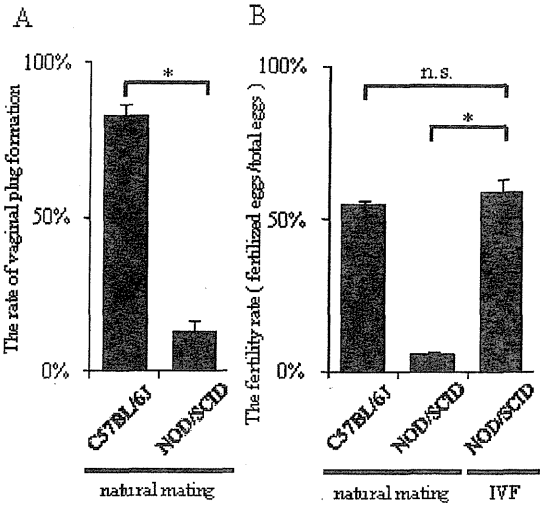

FIG. 1. The fertility rate of the NOD/SCID mice was improved by IVF. **A**) The rate of vaginal plug formation by natural mating in the NOD/SCID mice was significantly lower than that in the C57BL/6J mice. Data are presented as mean ± SEM. *$P < 0.01$. **B**) The fertility rate of the NOD/SCID mice obtained by natural mating was also significantly lower than that of the C57BL/6J mice, whereas IVF improved the fertility rate in the NOD/SCID mice to a level almost equal to that in the C57BL/6J mice. *$P < 0.01$. n.s., not significant.

Statistics

Data were expressed as ±SEM. Student *t*-test was used for statistical analysis of the differences between two groups, and the statistical significance of differences among multiple groups was determined by ANOVA and Tukey *t*-test.

RESULTS

Obtainment of a Sufficient Number of Fertilized Eggs of the NOD/SCID Mice by IVF

We first attempted to obtain fertilized eggs from the NOD/SCID and C57BL/6J mice by natural mating between 8-wk-old female mice and 10- to 12-wk-old male mice, and experiments of the rate of vaginal plug formation and fertility rate were repeated a total of three times; then we used 10 stud males and 10 females in a one-time experiment; and then one male and one female mated per cage.

The vaginal plug formation rate in the NOD/SCID mice was significantly lower (13.3%) than that in the C57BL/6J mice (83.3%; Fig. 1A). In fact, the fertility rate by natural mating in the NOD/SCID mice was also significantly lower (6.0%) than that in the C57BL/6J mice (55.1%; Fig. 1B). These observations prompted us to attempt to collect the fertilized eggs by IVF. The fertility rate was markedly elevated by IVF in the NOD/SCID mice (59.2%), to a level almost equal to that obtained by natural mating of the C57BL/6J mice (Fig. 1B). This result showed the possibility of obtaining a sufficient number of fertilized eggs, even from NOD/SCID mice, by using IVF instead of natural mating.

Construction of the CAG-EGFP Cassette

To examine the efficiency of the generation of the Tg mice, we tried to generate CAG-EGFP mice, so that the expression of the transgene in the whole body could be analyzed easily. We also selected this construct because overexpression of EGFP, even ubiquitously, has been reported to have no harmful effects

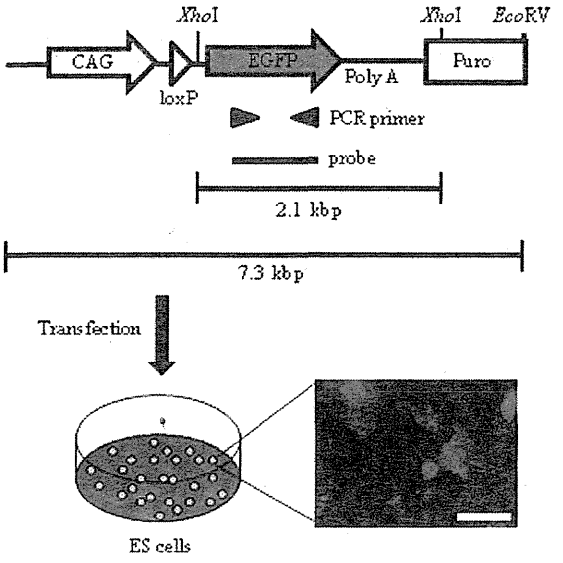

FIG. 2. The Z/EG expression construct expressing EGFP under the CAG promoter, whose size was 7.3 kbp. Primers for the PCR analysis and probe for the Southern blot analysis were set within the coding region of EGFP. Examination by a macrofluorescence microscopy system was employed to confirm EGFP expression in the ES cells after transfection. Puro^r indicates puromycin resistance gene. Bar = 100 μm.

on embryonic development. First, we produced the EGFP expression vector under the strong CAG promoter by Cre excision from the Z/EG plasmid, which consists of a *loxP*-flanked βgeo (*lacZ*/neomycin resistance) fusion gene and the EGFP gene [11]. Then, we inserted the puromycin resistance gene after the EGFP gene and linearized the plasmid, to obtain the CAG-EGFP Tg cassette. By transfecting the construct into murine ES cells, we found that the Tg cassette was actually efficient, and validated its use for the generation of Tg mice (Fig. 2).

Improved Rate of Development to the Two-Cell Stage by Delayed Timing of Microinjection

To compare the efficiency of the microinjection into the NOD/SCID eggs compared with that into the C57BL/6J eggs, we first injected the EGFP construct into the eggs of both strains at 8 h after the IVF, the usual interval employed for the C57BL/6J mice, and analyzed the efficiency by morphologic examination. Although the fertilized eggs of the C57BL/6J mice developed efficiently to two-cell-stage embryos (Fig. 3, A–C), clear formation of the pronuclei was not observed in the fertilized eggs of the NOD/SCID mice, and most of the eggs did not develop normally into two-cell-stage embryos, with a high incidence of apparent morphological abnormalities (Fig. 3, D–F). This result suggests that the embryo development of the NOD/SCID mice was slower than that of the C57BL/6J mice. It has been reported previously that the embryos of some

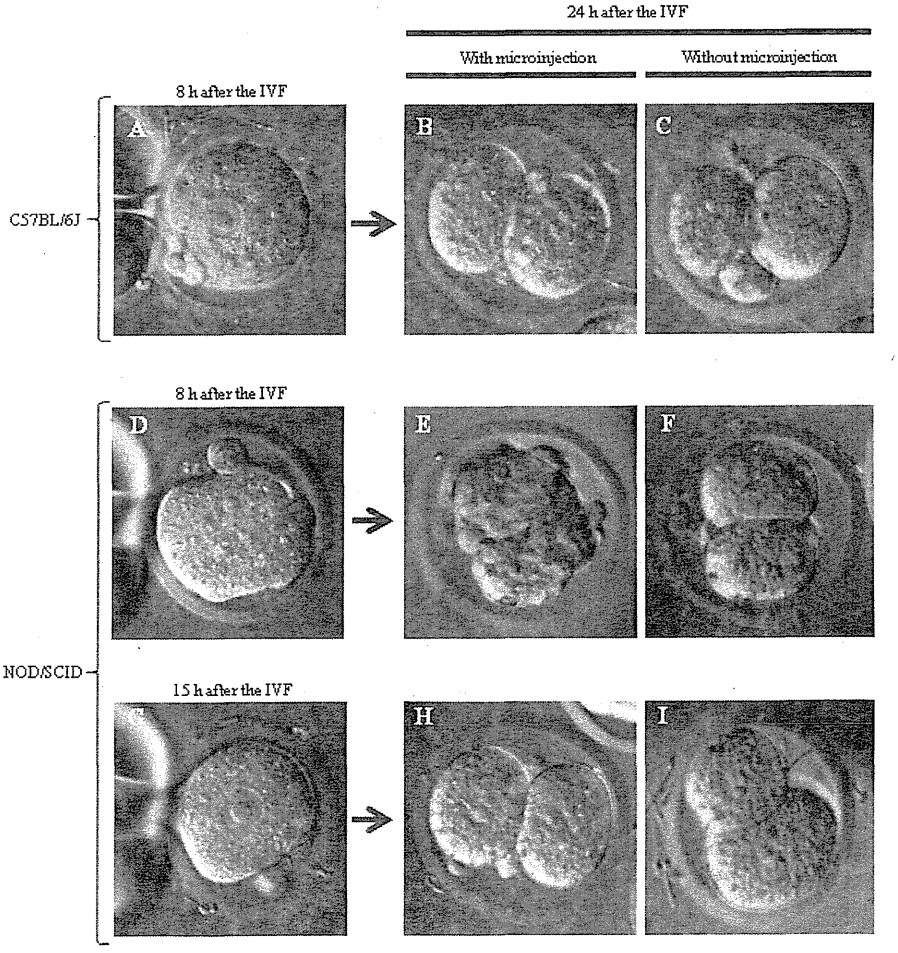

FIG. 3. Two-cell-stage embryos with or without microinjection. **A**) A representative fertilized egg of the C57BL/6J mouse at 8 h after the IVF. **B** and **C**) A representative two-cell-stage embryo of the C57BL/6J mouse obtained with (**B**) and without (**C**) microinjection at 24 h after the IVF. **D**) A representative fertilized egg of the NOD/SCID mouse at 8 h after the IVF. **E** and **F**) A representative two-cell-stage embryo of the NOD/SCID mouse obtained with (**E**) and without (**F**) microinjection at 24 h after the IVF. **G**) A representative fertilized egg of the NOD/SCID mouse at 15 h after the IVF. **H** and **I**) A representative two-cell-stage embryo of the NOD/SCID mouse obtained with (**H**) and without (**I**) microinjection at 24 h after the IVF. Original magnification ×520.

TABLE 1. The tolerance of the NOD/SCID embryos to microinjection.

Interval between IVF and microinjection	No. of injected fertilized eggs	No. of 2-cell stage embryos*	Ratio
8 h	364	116	31.9%
15 h	382	312	81.7%

* Developmental status was examined 9 h after the microinjection.

TABLE 2. The birthrate of microinjected cells.

Interval between IVF and microinjection	No. of 2-cell stage embryos 9 h after microinjection	Newborns	Ratio
8 h	116	0	0.0%
15 h	312	83	26.6%

mouse strains develop more slowly than those of other strains of mice [14], and the pronuclei have been shown to become well defined only by 16–20 h after fertilization in some strains [15]. Therefore, we delayed the microinjection to 15 h after the IVF, and found clear pronuclei in the fertilized eggs of the NOD/SCID mice. Moreover, a sufficient number of the eggs developed into two-cell-stage embryos without any morphological abnormalities (Fig. 3, G–I).

Following the microinjection at 8 h after the IVF, 116 (31.9%) of the 364 injected fertilized eggs developed into two-cell-stage embryos. By contrast, following the microinjection at 15 h after the IVF, 312 (81.7%) of the 382 injected fertilized eggs successfully developed into two-cell-stage embryos (Table 1).

Improved Birth Rate with Delayed Timing of the Microinjection

To examine the effect of delayed timing of the microinjection on development after the two-cell stage, we compared the birth rate between the early and delayed injections. Following the microinjection at 8 h after the IVF, no newborns were obtained from 116 injected fertilized eggs (0.0%). By contrast, following the microinjection at 15 h after the IVF, 83 newborns were successfully obtained from 312 injected fertilized eggs (26.6%; Table 2). This result showed that delaying the timing of the microinjection—i.e., to 15 h after the IVF—markedly improved the efficiency of the microinjection in the NOD/SCID mice.

Generation of CAG-EGFP Tg Mice on an NOD/SCID Background

To examine the integration of the injected gene fragment into the genomic DNA, we first performed PCR analysis. As expected, a 361-bp band from EGFP was detected from the genomic DNA in 7 of 83 newborns (Fig. 4A). We then performed Southern blotting after digestion with *Xho*I. Again, as expected, a 2.1-kbp band from EGFP was detected (Fig. 4B). Actually, examination by the macrofluorescence microscopy system revealed the expression of EGFP throughout the body (Fig. 4C), confirming that these newborns were definitely CAG-EGFP Tg mice.

Examination of the Tg mice by the macrofluorescence microscopy system revealed expression of EGFP in various organs (Fig. 5). These results showed that CAG-EGFP Tg mice were successfully generated on the NOD/SCID background by means of microinjection.

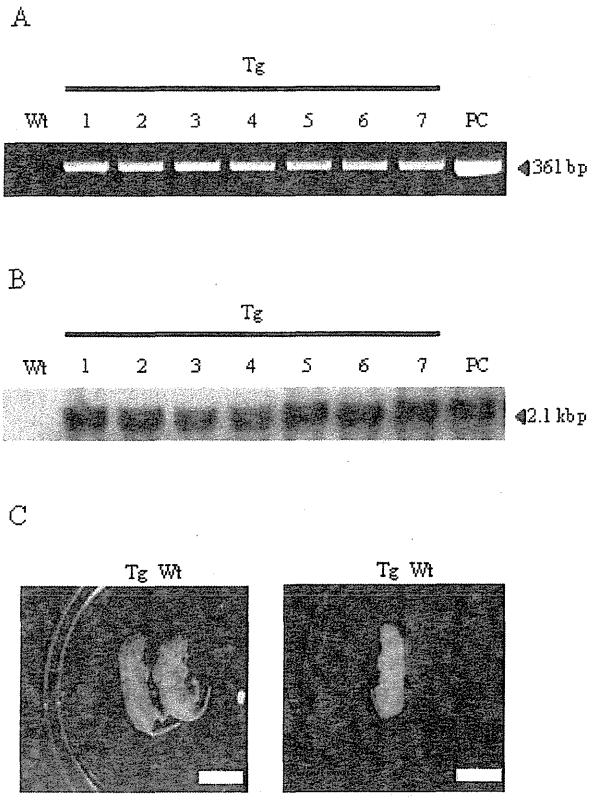

FIG. 4. Generation of CAG-EGFP Tg mice on an NOD/SCID background. The position of the PCR primers and the probe for the Southern blot analysis are indicated in Figure 2. **A**) A PCR analysis of the genotype. Wt, non-Tg mice; No. 1, No. 2, No. 3, No. 4, No. 5, No. 6, and No. 7, CAG-EGFP Tg mice showing a 361-bp band amplified by PCR; PC, the construct used for the positive control. **B**) Southern blot analysis after digestion with *Xho*I. Wt, non-Tg mice; No. 1, No. 2, No. 3, No. 4, No. 5, No. 6, and No. 7, CAG-EGFP Tg mice showing a 2.1-kbp band. **C**) Microscopic examination of the F(0) mice (left) and detection of EGFP (right). Bar = 10 mm.

Confirmation of Germ-Line Transmission

To confirm the germ-line transmission in the Tg mice, we generated F(1) mice by natural mating. We succeeded in obtaining F(1) mice, and all PCR analysis (Fig. 6A), Southern blot analysis (Fig. 6B), and macrofluorescence microscopy (Fig. 6C) confirmed the germ-line transmission to the Tg mice.

DISCUSSION

In this study, transgenic immunodeficient mice were obtained within 3 mo, at physical containment level P1, by means of IVF to obtain a sufficient number of fertilized eggs of the NOD/SCID mice, and then delayed microinjection of the transgene into the fertilized eggs.

To analyze the biological functions of foreign genes in vivo, many investigators have generated transgenic mice by the microinjection technique. In this technique, a construct is injected into the pronucleus of a fertilized egg by insertion of a microinjection pipette. By transferring these fertilized eggs into pseudopregnant recipient females (0.5 days after coitus) previously mated with vasectomized males, Tg newborns are obtained by natural birth or cesarean delivery [16–18]. This method does not require the use of infectious virus vectors, and can thus be completed at physical containment level P1. The

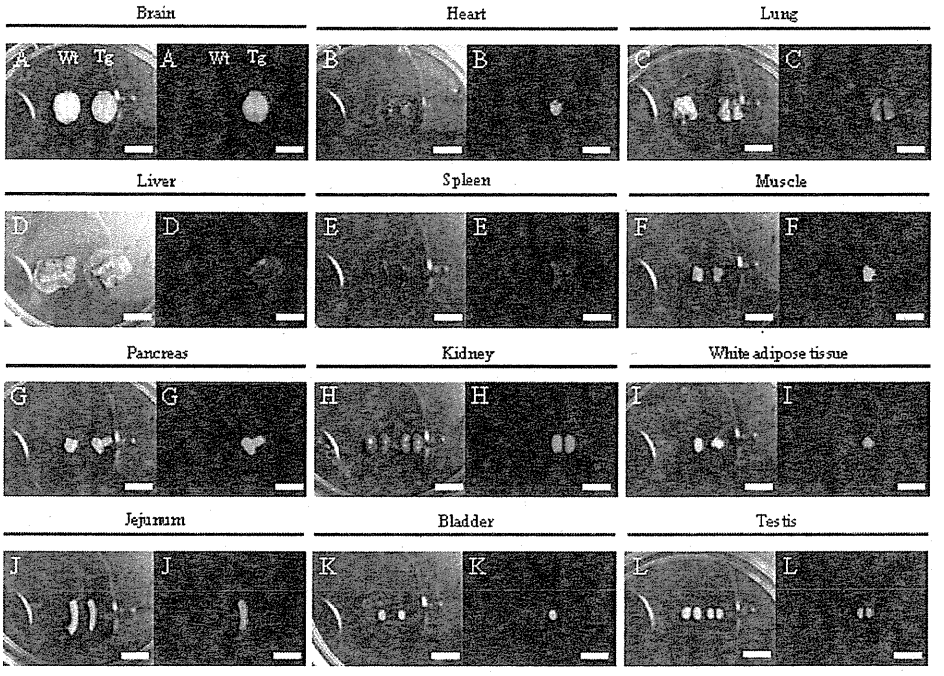

FIG. 5. Expression of EGFP in various organs. Examination macrofluorescence microscopy system revealed expression of EGFP in the brain (**A**), heart (**B**), lung (**C**), liver (**D**), spleen (**E**), muscle (**F**), pancreas (**G**), kidney (**H**), white adipose tissue (**I**), jejunum (**J**), bladder (**K**), and testis (**L**). Bar = 10 mm.

efficiency of Tg mouse generation by microinjection, however, depends on the mouse strain, and it is difficult to generate Tg mice from some strains of mice [14]; for instance, there has been no report to date of the generation of transgenic mice on an NOD/SCID background by microinjection.

Although NOD/SCID mice are potentially among the most powerful tools for generating humanized mice because of their immune tolerance, generation of Tg mice on this background is known to be extremely difficult. Three methods have mainly been reported until now: the lentiviral vector method; backcrossing already generated Tg mice on a wild-type

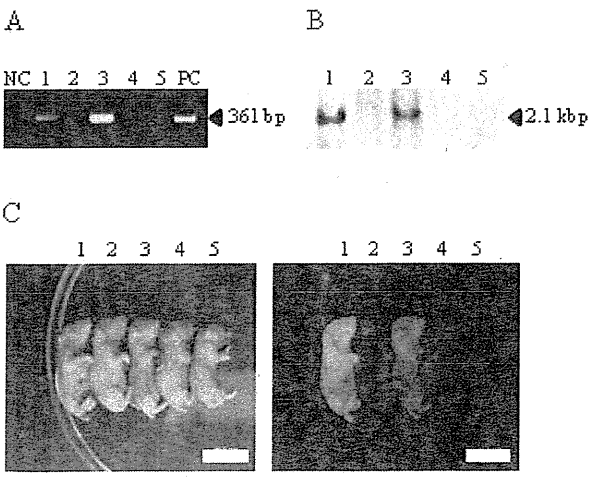

FIG. 6. Confirmation of the germ-line transmission in the F(0) mice. All of the PCR analysis (**A**), Southern blot analysis (**B**), and macrofluorescence microscopy (**C**) indicated that among the five F(1) mice, nos. 1 and 3 were Tg mice. NC, negative control; PC, positive control. Bar = 10 mm.

background with an NOD/SCID strain, which could be combined with the speed congenics method for period shortening; and backcrossing already generated Tg mice on an NOD background with the NOD/SCID strain. Lentivirus is one of the retroviruses, and it has the distinct characteristic of being capable of infecting both dividing and nondividing cells; this is the reason a lentiviral vector containing a strong promoter has become one of the most popular gene delivery vehicles [19, 20]. After infecting zygotes with a lentivirus expressing the gene of interest, the zygotes are cultured overnight in medium drops (37°C, 5% CO_2). Two-cell-stage embryos are then transferred into the ampullae (oviduct transfer) of pseudopregnant recipient females (0.5 days after coitus) previously mated with vasectomized males. Newborns are obtained by natural birth or cesarean delivery [9]. The lentiviral vector infection method can generate Tg within 3 mo, almost as quickly as the microinjection system. All of the manipulations using the lentivirus, however, need to be performed at physical containment levels P2 or P3, because of the high potential of the virus to infect human cells. Moreover, the Tg mice, including the offspring, generated by this method also need to be maintained at physical containment level P2 or P3. Furthermore, genetic mosaicism has been reported to occur when viral constructs are used [20–25]. By contrast, in the method used in this study, the manipulations are performed at physical containment level P1, and the Tg mice, including the offspring, can also be maintained at physical containment level P1, showing that the microinjection system can overcome the most important drawback of the lentiviral infection method.

In the second method, Tg mice are generated on a wild-type background by microinjection in advance, followed by backcrossing with an immunodeficient strain [10]. Although this method can be performed at physical containment level P1, backcrossing by natural mating requires around 2 yr: 90 days

(period of Tg generation) + ([20 days {period between mating and birth} + 20 days {period between birth and weaning} + 40 days {period between weaning and reaching the breeding age}] × 8 [mating times for backcrossing]). Even if this method were combined with the speed congenics method, which enables generation of mice on a certain background in an accelerated manner, it would still take four backcrossings and require at least about 1 yr [26, 27]. In this study, the Tg mice generated by direct microinjection into fertilized eggs of the NOD/SCID mice needed no backcrossing. The microinjection system again has an advantage over backcrossing, in that Tg mice with an immunodeficient background can be generated directly within 3 mo.

Third, it may also be possible to generate Tg mice directly on an NOD background, followed by backcrossing with NOD/SCID mice, which are homozygous for the *scid* mutation on an NOD background. This strategy, however, still requires two backcrossings. Furthermore, insulitis occurring at the age of 4 wk causes severe diabetes in the NOD mice [28, 29], which is considered to be a potential barrier against backcrossing, although the NOD/SCID mice do not develop diabetes. By contrast, the microinjection system can also overcome this drawback.

In our newly developed method, one of the key factors that enabled us to efficiently generate Tg mice directly on the NOD/SCID background mice was IVF. In fact, a sufficient number of fertilized eggs were successfully obtained, even from the NOD/SCID mice. Another important factor was the delayed timing of the microinjection. Previous studies suggest that the genetic background of the egg donor has an influence on the overall efficiency of production of Tg mice. The FVB/N inbred mice and the B6D2/F2 hybrid mice have consistently been demonstrated to show the highest efficiency [14, 30–34]. It is speculated that slower development of pronuclei may be associated with a reduced efficiency in some strains, because less visible pronuclei are difficult to inject, and the zygotes can be damaged by the injector. These considerations suggest that delaying of the timing of the microinjection may be required in such strains [14]. In fact, pronuclei of the NOD/SCID eggs developed much slower than those of the C57BL/6J eggs; it took as long as 15 h until they became clearly visible after the IVF. Moreover, although most of the fertilized eggs in NOD/SCID mice injected at 8 h after the IVF did not develop normally into two-cell-stage embryos with morphological abnormalities, the eggs injected at 15 h after the IVF efficiently developed into two-cell-stage embryos without morphological abnormalities.

In conclusion, we have established an improved strategy, based on the conventional microinjection technique, to generate stable Tg mice on an NOD/SCID background. The technique, involving a combination of IVF and delayed timing of the microinjection, enabled us to generate Tg mice at physical containment level P1 within 3 mo, thereby overcoming the problems associated with the previously described methods of lentiviral infection and backcrossing. This strategy is expected to greatly contribute to improved efficiency of generation of humanized mice.

ACKNOWLEDGMENTS

We thank Dr. Andras Nagy of the Samuel Lunenfeld Research Institute Mount Sinai Hospital, and Dr. Jun Ohgane and Dr. Kunio Shiota of the Laboratory of Cellular Biochemistry, Animal Resource Sciences/Veterinary Medical Sciences, University of Tokyo, for providing the CAG promoter/enhancer EGFP cassette. We also thank Hitoshi Miyauchi of the Institute for Virus Research, Kyoto University, for his valuable technical assistance.

REFERENCES

1. Krimpenfort P, Rudenko G, Hochstenbach F, Guessow D, Berns A, Ploegh H. Crosses of two independently derived transgenic mice demonstrate functional complementation of the genes encoding heavy (HLA-B27) and light (beta 2-microglobulin) chains of HLA class I antigens. EMBO J 1987; 6:1673–1676.
2. Tepper RI, Levinson DA, Stanger BZ, Campos-Torres J, Abbas AK, Leder P. IL-4 induces allergic-like inflammatory disease and alters T cell development in transgenic mice. Cell 1990; 62:457–467.
3. Yamamoto T. Animal model of systemic sclerosis. J Dermatol 2010; 37: 26–41.
4. Weissman A, Gotlieb L, Colgan T, Jurisicova A, Greenblatt EM, Casper RF. Preliminary experience with subcutaneous human ovarian cortex transplantation in the NOD/SCID mouse. Biol Reprod 1999; 60:1462–1467.
5. Suemizu H, Hasegawa M, Kawai K, Taniguchi K, Monnai M, Wakui M, Suematsu M, Ito M, Peltz G, Nakamura M. Establishment of a humanized model of liver using NOD/Shi-scid IL2Rgnull mice. Biochem Biophys Res Commun 2008; 377:248–252.
6. Bosma GC, Custer RP, Bosma MJ. A severe combined immunodeficiency mutation in the mouse. Nature 1983; 301:527–530.
7. Greiner DL, Shultz LD, Yates J, Appel MC, Perdrizet G, Hesselton RM, Schweitzer I, Beamer WG, Shultz KL, Pelsue SC, Leif JH, Rajan TV. Improved engraftment of human spleen cells in NOD/LtSz-scid/scid mice as compared with C.B-17-scid/scid mice. Am J Pathol 1995; 146:888–902.
8. Ito M, Hiramatsu H, Kobayashi K, Suzue K, Kawahata M, Hioki K, Ueyama Y, Koyanagi Y, Sugamura K, Tsuji K, Heike T, Nakahata T. NOD/SCID/gamma(c)(null) mouse: an excellent recipient mouse model for engraftment of human cells. Blood 2002; 100:3175–3182.
9. Punzon I, Criado LM, Serrano A, Serrano F, Bernad A. Highly efficient lentiviral-mediated human cytokine transgenesis on the NOD/scid background. Blood 2004; 103:580–582.
10. Camacho RE, Wnek R, Shah K, Zaller DM, O'Reilly RJ, Collins N, Fitzgerald-Bocarsly P, Koo GC. Intra-thymic/splenic engraftment of human T cells in HLA-DR1 transgenic NOD/scid mice. Cell Immunol 2004; 232:86–95.
11. Novak A, Guo C, Yang W, Nagy A, Lobe CG. Z/EG, a double reporter mouse line that expresses enhanced green fluorescent protein upon Cre-mediated excision. Genesis 2000; 28:147–155.
12. Yagi T, Tokunaga T, Furuta Y, Nada S, Yoshida M, Tsukada T, Saga Y, Takeda N, Ikawa Y, Aizawa S. A novel ES cell line, TT2, with high germline-differentiating potency. Anal Biochem 1993; 214:70–76.
13. Carroll J, Warnes G, Matthews C. Increase in digyny explains polyploidy after in-vitro fertilization of frozen-thawed mouse oocytes. J Reprod Fertil 1989; 85:489–494.
14. Auerbach AB, Norinsky R, Ho W, Losos K, Guo Q, Chatterjee S, Joyner AL. Strain-dependent differences in the efficiency of transgenic mouse production. Transgenic Res 2003; 12:59–69.
15. Hogan B, Costantini F, Lacy E. Manipulating the Mouse Embryo: A Laboratory Manual, trans. Kazuya Y, Yutaka T, Tsuneatsu M, Yoichiro I. Tokyo, Japan: Kindai-Shuppan; 1986:17–75.
16. Costantini F, Lacy E. Introduction of a rabbit beta-globin gene into the mouse germ line. Nature 1981; 294:92–94.
17. Harbers K, Jahner D, Jaenisch R. Microinjection of cloned retroviral genomes into mouse zygotes: integration and expression in the animal. Nature 1981; 293:540–542.
18. Brinster RL, Chen HY, Trumbauer M, Senear AW, Warren R, Palmiter RD. Somatic expression of herpes thymidine kinase in mice following injection of a fusion gene into eggs. Cell 1981; 27:223–231.
19. Naldini L, Blomer U, Gallay P, Ory D, Mulligan R, Gage FH, Verma IM, Trono D. In vivo gene delivery and stable transduction of nondividing cells by a lentiviral vector. Science 1996; 272:263–267.
20. Lois C, Hong EJ, Pease S, Brown EJ, Baltimore D. Germline transmission and tissue-specific expression of transgenes delivered by lentiviral vectors. Science 2002; 295:868–872.
21. Kotnik K, Popova E, Todiras M, Mori MA, Alenina N, Seibler J, Bader M. Inducible transgenic rat model for diabetes mellitus based on shRNA-mediated gene knockdown. PLoS One 2009; 4:e5124.
22. Park F. Lentiviral vectors: are they the future of animal transgenesis? Physiol Genomics 2007; 31:159–173.
23. Dann CT, Alvarado AL, Hammer RE, Garbers DL. Heritable and stable gene knockdown in rats. Proc Natl Acad Sci U S A 2006; 103:11246–11251.
24. Van den Brandt J, Wang D, Kwon SH, Heinkelein M, Reichardt HM. Lentivirally generated eGFP-transgenic rats allow efficient cell tracking in vivo. Genesis 2004; 39:94–99.

25. Scott BB, Lois C. Generation of tissue-specific transgenic birds with lentiviral vectors. Proc Natl Acad Sci U S A 2005; 102:16443–16447.
26. Markel P, Shu P, Ebeling C, Carlson GA, Nagle DL, Smutko JS, Moore KJ. Theoretical and empirical issues for marker-assisted breeding of congenic mouse strains. Nat Genet 1997; 17:280–284.
27. Wong GT. Speed congenics: applications for transgenic and knock-out mouse strains. Neuropeptides 2002; 36:230–236.
28. Kataoka S, Satoh J, Fujiya H, Toyota T, Suzuki R, Itoh K, Kumagai K. Immunologic aspects of the nonobese diabetic (NOD) mouse: abnormalities of cellular immunity. Diabetes 1983; 32:247–253.
29. Leiter EH. The NOD mouse: a model for analyzing the interplay between heredity and environment in development of autoimmune disease. ILAR News 1993; 35:4–14.
30. Brinster RL, Chen HY, Trumbauer ME, Yagle MK, Palmiter RD. Factors affecting the efficiency of introducing foreign DNA into mice by microinjecting eggs. Proc Natl Acad Sci U S A 1985; 82:4438–4442.
31. Taketo M, Schroeder AC, Mobraaten LE, Gunning KB, Hanten G, Fox RR, Roderick TH, Stewart CL, Lilly F, Hansen CT. FVB/N: an inbred mouse strain preferable for transgenic analyses. Proc Natl Acad Sci U S A 1991; 88:2065–2069.
32. Mann JR, McMahon AP. Factors influencing frequency production of transgenic mice. Methods Enzymol 1993; 225:771–781.
33. Paris D, Toyama PM, Sinet PM, Kamoun P, London J. A comparison between an inbred strain and hybrid lines to generate transgenic mice. Mouse Genome 1995; 93:21–23.
34. Osman GE, Jacobson DP, Li SW, Hood LE, Liggitt HD, Ladiges WC. SWR: an inbred strain suitable for generating transgenic mice. Lab Anim Sci 1997; 47:167–171.

Available online at www.sciencedirect.com
ScienceDirect
Metabolism Clinical and Experimental 60 (2011) 617–628
Metabolism
Clinical and Experimental
www.metabolismjournal.com

Ezetimibe decreases SREBP-1c expression in liver and reverses hepatic insulin resistance in mice fed a high-fat diet

Tomonori Muraoka[a], Kazutaka Aoki[a], Tomoyuki Iwasaki[a], Kazuaki Shinoda[a], Akinobu Nakamura[a], Hiroyuki Aburatani[b], Shuuichi Mori[c], Kumpei Tokuyama[c], Naoto Kubota[d], Takashi Kadowaki[d], Yasuo Terauchi[a,*]

[a]*Department of Endocrinology and Metabolism, Yokohama City University Graduate School of Medicine, Yokohama 236-0004, Japan*
[b]*Genome Science Division, Research Center for Advanced Science and Technology, University of Tokyo, Tokyo 153-8904, Japan*
[c]*Graduate School of Comprehensive Human Sciences, University of Tsukuba, Tsukuba 305-0006, Japan*
[d]*Department of Metabolic Diseases, Graduate School of Medicine, University of Tokyo, Tokyo 113-8655, Japan*

Received 21 December 2009; accepted 7 June 2010

Abstract

Ezetimibe inhibits intestinal cholesterol absorption, thereby reducing serum cholesterol. Recent studies suggest that ezetimibe affects liver steatosis and insulin resistance. We investigated the impact of ezetimibe on insulin sensitivity and glucose metabolism in C57BL/6 mice. We analyzed 4 mouse groups fed the following diets: normal chow (4% fat) for 12 weeks, normal chow for 10 weeks followed by normal chow plus ezetimibe for 2 weeks, high-fat chow (32% fat) for 12 weeks, and high-fat chow for 10 weeks followed by high-fat chow plus ezetimibe for 2 weeks. In the normal chow + ezetimibe group, ezetimibe had no impact on body weight, fat mass, lipid metabolism, liver steatosis, glucose tolerance, or insulin sensitivity. In the high-fat chow + ezetimibe group, ezetimibe had no impact on body weight or fat mass but significantly decreased serum low-density lipoprotein cholesterol, triglyceride, and glutamate pyruvate transaminase levels; liver weight; hepatic triglyceride content; and hepatic cholesterol content and increased the hepatic total bile acid content. In association with increases in IRS-2 and Akt phosphorylation, ezetimibe ameliorated hepatic insulin resistance in the high-fat chow + ezetimibe group, but had no effect on insulin sensitivity in primary cultured hepatocytes. A DNA microarray and Taqman polymerase chain reaction revealed that ezetimibe up-regulated hepatic SREBP2 and SHP expression and down-regulated hepatic SREBP-1c expression. SHP silencing mainly in the liver worsened insulin resistance, and ezetimibe protected against insulin resistance induced by down-regulation of SHP. Ezetimibe down-regulated SREBP-1c in the liver and reversed hepatic insulin resistance in mice fed a high-fat diet.

1. Introduction

Ezetimibe is a novel sterol absorption inhibitor that blocks Niemann-Pick C1-Like 1 (NPC1L1)–mediated cholesterol absorption in the apical brush border membrane of jejunal enterocytes [1]. NPC1L1 null mice were completely resistant to high-cholesterol-diet–induced hypercholesterolemia, with plasma lipoprotein and hepatic cholesterol profiles similar to those of wild-type mice treated with ezetimibe [2]. Ezetimibe prevented lipid-rich-diet–induced increase in biliary cholesterol in hamsters [3]. Recently, potential consequences of ezetimibe relative to metabolism of other nutrients have been investigated. In animal experiments, ezetimibe reversed diet-induced obesity [4,5], liver steatosis [4-7], and insulin resistance [6]. In humans, in addition to the effect of ezetimibe on lowering serum low-density lipoprotein (LDL) cholesterol [8], its potential effects on liver steatosis [9] and insulin resistance [10] have been reported. Nevertheless, the mechanism whereby ezetimibe achieves these favorable effects on insulin sensitivity remains unclear. These circumstances prompted us to investigate the effects of ezetimibe on insulin sensitivity and glucose metabolism using high-fat-diet–induced C57BL/6 obese mice to pursue the possibility of new mechanisms explaining these beneficial effects.

* Corresponding author. Tel.: +81 45 787 2639.
E-mail address: terauchi@yokohama-cu.ac.jp (Y. Terauchi).

0026-0495/$ – see front matter © 2011 Elsevier Inc. All rights reserved.
doi:10.1016/j.metabol.2010.06.008

2. Materials and methods

2.1. Chemicals

Ezetimibe is a novel sterol absorption inhibitor that blocks NPC1L1-mediated cholesterol/phytosterol absorption in the apical brush border membrane of jejunal enterocytes, as described previously [1]. The Schering-Plough Research Institute provided us with ezetimibe.

2.2. Animals and diet protocol

Male C57BL/6 mice (7 weeks of age) (Japan SLC, Shizuoka, Japan) were fed a normal chow diet (Type MF; Oriental Yeast, Tokyo, Japan) for 1 week and were then divided into 4 groups that were each fed a specific diet for the next 12 weeks. We thus analyzed 4 mouse groups, namely, mice fed a normal chow diet for 12 weeks (NC), mice fed a normal chow diet for 10 weeks followed by normal chow diet containing 0.005% wt/wt ezetimibe for 2 weeks (NC + Ez), mice fed a high-fat chow (High-Fat Diet 32; CLEA Japan, Tokyo, Japan) for 12 weeks (HF), and mice fed a high-fat chow for 10 weeks followed by high-fat chow containing 0.005% wt/wt ezetimibe for 2 weeks (HF + Ez). Cholesterol absorption is inhibited by more than 90% at ezetimibe doses of more than 3 mg/kg in apolipoprotein E–knockout mice [11]. The target doses of 0.005% wt/wt ezetimibe mixed in either normal chow or high-fat chow corresponded to a dose of 3 mg/kg body weight in the C57BL/6J mice. The nutrient compositions of the chows are described in Table 1. The mice were given free access to water and food until the start of the experiments. The experiments were approved by the Ethical Committee for Animal Experimentation of Yokohama City Medical University, and the animals were maintained according to standard animal care procedures based on institutional guidelines.

2.3. Measurement of lipids and bile acid

The extraction of lipids from liver tissue was performed as described by Folch et al [12]. Plasma lipoproteins were analyzed using an online dual enzymatic method for the simultaneous quantification of cholesterol and triglycerides (TGs) using high-performance liquid chromatography at Skylight Biotech (Akita, Japan), according to the procedure reported by Usui et al [13]. The total bile acid level in the serum was determined by using enzymatic methods at SRL (Tokyo, Japan). Bile acid in the liver was extracted using the ethanol-thermal method, and the bile acid content was determined using enzymatic methods at Skylight-Biotec according to the procedure reported by Udagawa et al [14] with slight modifications.

Table 1
Nutritional components of Type MF and High-Fat Diet 32

	Type MF	High-Fat Diet 32
Moisture (g/100 g)	7.8	6.9
Content of crude protein (g/100 g)	23.8	25.0
Content of crude fat (g/100 g)	3.7	32.4
Content of crude ash (g/100 g)	6.1	4.0
Content of crude fiber (g/100 g)	3.2	2.9
Nitrogen-free extract (g/100 g)	54.0	28.8
Cholesterol content (mg/100 g)	75	12.9
Calorie (kcal/100 g)	357	507.6

2.4. Histology of the liver

To study the liver histology, the livers were dissected and fixed in buffered neutral formalin (10%). The fixed-tissue blocks were embedded in paraffin, and 4-μm paraffin sections were stained using the standard hematoxylin and eosin staining procedure.

2.5. Oral glucose tolerance test

Each group of mice was given an oral glucose tolerance test (1.5 mg of glucose per gram of body weight after 18 hours of fasting). The glucose levels were measured at 0, 15, 30, 60, and 120 minutes using whole blood obtained from the tail vein and a portable blood glucose analyzer (Glutest Neo; Sanwa Chemical, Nagoya, Japan); the insulin levels were measured at 0, 15, and 30 minutes using an enzyme-linked immunosorbent assay kit (Morinaga, Kanagawa, Japan), as previously described [15].

2.6. Insulin tolerance test

Each group of mice was given an insulin tolerance test. Mice were given free access to food and were then intraperitoneally injected with 0.75 mU of insulin per gram of body weight. The glucose levels were then measured at 0, 15, 30, 60, and 120 minutes using whole blood obtained from the tail vein and a portable blood glucose analyzer (Glutest Neo).

2.7. Hyperinsulinemic-euglycemic clamp study

Clamp studies were performed as described previously [16-18]. Briefly, 2 to 3 days before the study, an infusion catheter was inserted into the right jugular vein under general anesthesia with sodium pentobarbital. Studies were performed on mice under conscious and unstressed conditions after a 6-hour fast. A primed continuous infusion of insulin (Humulin R; Eli Lilly and Company, Indianapolis, IN, USA) was given (5.0 mU/[kg min]), and the blood glucose concentration, monitored every 5 minutes, was maintained at 120 mg/dL through the administration of glucose (5 g of glucose per 10 mL enriched to approximately 20% with [6,6-2H2]glucose [Sigma, Tokyo, Japan]) for 120 minutes. Blood was sampled via tail tip bleeds at 90, 105, and 120 minutes to determine the rate of glucose disappearance (Rd). Rd was calculated using non–steady-state equations, and endogenous glucose production (EGP) was calculated as the difference between Rd and the exogenous glucose infusion rate (GIR).

2.8. In vivo IRS-1/2 and Akt phosphorylation

The monoclonal antiphosphotyrosine antibody (anti-PY), polyclonal anti–IRS-1 antibody (anti–IRS-1), and polyclonal anti–IRS-2 antibody (anti–IRS-2) were purchased from Upstate Biotechnology (Lake Placid, NY, USA). Rabbit polyclonal anti–phospho-Akt antibody (anti-pAkt) recognizing phosphorylated Ser-473 of Akt1 and rabbit anti-Akt antibody (anti-Akt) were purchased from Cell Signaling Technology (Beverly, MA). Mice in the HF and HF + Ez groups were starved for 24 hours, anesthetized with pentobarbital, and injected with 15 units of regular human insulin (Humulin R) or saline into the inferior vena cava. Seventy seconds later, the livers were excised and homogenized in ice cold buffer A (25 mmol/L Tris-HCl [pH 7.4], 10 mmol/L Na_3VO_4, 10 mmol/L NaPPi, 100 mmol/L NaF, 10 mmol/L EDTA, 10 mmol/L EGTA, and 1 mmol/L phenylmethylsulfonyl fluoride). Lysates were prepared by centrifugation (15 000 rpm, 20 minutes, 4°C). Immunoprecipitation analyses for either IRS-1 or IRS-2 and Western blot analyses for Akt and pAkt were then performed. To detect the immunoprecipitation of either IRS-1 or IRS-2 and their phosphorylation, liver extracts were incubated with specific antibodies against either IRS-1 or IRS-2 at 4°C overnight and then with protein G–Sepharose for 2 hours at 4°C. After washing 3 times with buffer A, the immunocomplexes were resolved on 7% sodium dodecyl sulfate polyacrylamide gel electrophoresis. The phosphorylated or total protein was then analyzed using immunoblotting with specific antibodies against either IRS-1 or IRS-2 and a phosphotyrosine antibody. Akt activity was expressed as the ratio of the intensity of pAkt to Akt.

2.9. RNA preparation and microarray analysis of messenger RNA levels in the liver

Mice in the HF and HF + Ez groups were subjected to fasting for 24 hours. Total RNA was prepared from portions of the liver using Isogen Reagent (NipponGene, Tokyo, Japan) according to the manufacturer's instructions. RNA was further purified using a NucleoSpin RNA II column (Macherey-Nagel, Duren, Germany), and RNA quality was assessed after electrophoresis in a 1% agarose gel. GeneChip assays were then performed, as previously described [18]. Briefly, double-strand standard complementary DNA with a T7 promoter was synthesized from 5 μg of total RNA using the SuperScript choice system (Invitrogen-Life Technologies, Carlsbad, CA, USA). Approximately 50 μg of biotin-labeled complementary RNA was synthesized using in vitro transcription with T7 polymerase. After purification and fragmentation, complementary RNA was hybridized to the oligonucleotide microarray (Mouse Genome 430 2.0 Array; Affymetrix, Santa Clara, CA, USA). The scanned images were interpreted using GeneChip Operating Software 1.4 (Affymetrix) to generate a score representing the expression level of each gene. The microarray data have been deposited in the Gene Expression Omnibus public database.

2.10. Taqman polymerase chain reaction

Total RNA was prepared as mentioned above. The messenger RNA levels in the liver were quantitatively analyzed using fluorescence-based reverse transcriptase polymerase chain reaction (PCR). The reverse transcription mixture was amplified using specific primers and an ABI Prism 7500 sequence detector equipped with a thermocycler. The primers were purchased from Applied Biosystems (Foster City, CA). The relative expression levels were compared after normalization to β-actin [19].

2.11. Establishment of primary cultured hepatocytes and in vitro Akt phosphorylation experiment

Mice were anesthetized by the intraperitoneal administration of pentobarbital (40 mg/kg). Mouse hepatocytes were then isolated by the perfusion of collagenase through the abdominal vein, as previously described [20,21]. Briefly, the liver was perfused with a calcium-free Hanks HEPES buffer containing EGTA, followed by perfusion with Hanks HEPES buffer containing collagenase (0.1%). The "softened" liver was then excised, and the hepatocytes were separated from the connective tissue by filtering through macroporous filters (150 mesh; Ikemoto Scientific Technology, Tokyo, Japan). To remove nonparenchymal cells, the hepatocytes were washed with Williams medium E in Hanks buffer by repeated centrifugation for 3 minutes (each time) at 50*g*. The cell pellet was resuspended in Williams medium E containing streptomycin (100 μg/mL), penicillin (100 U/mL), and fetal bovine serum (10%); and the cell suspension was seeded into 24-well collagen-coated plates. The cells were cultured at 37°C under 5% CO_2 humidified air. After overnight incubation, the cells were washed with phosphate-buffered saline (PBS); and the buffer was changed to glucose-free Hanks solution, a substrate for gluconeogenesis, as previously described [22]. The cells were washed with PBS and then treated with ezetimibe (25 μmol/L) or dimethyl sulfoxide in medium for 48 hours, followed by treatment with insulin (10 nmol/L) or PBS for 5 minutes, as previously described [4]. The cells were lysed and subjected to Western blot analysis, as described above. Akt activity was expressed as the ratio of the intensity of pAkt to Akt.

2.12. Preparations of small interfering RNA and small interfering RNA treatment

Synthetic small interfering RNA (siRNA) was purchased from Takara Bio (Shiga, Japan). Sequences of the sense and anti-sense strands of siRNA were 5′-CGGACUUCCUUGCUUUGGATT-3′ and 5′-UCCAAAGCAAGGAACUCGTT-3′, respectively. Synthetic siRNAs were delivered in vivo using a modified hydrodynamic transfection method [23]. Mice fed a high-fat chow for 10 weeks were fasted 12 hours before hydrodynamic injection. Fifty micrograms siRNA dissolved in 2 mL Ringer buffer was rapidly injected into the tail vein, and then mice were immediately refed either

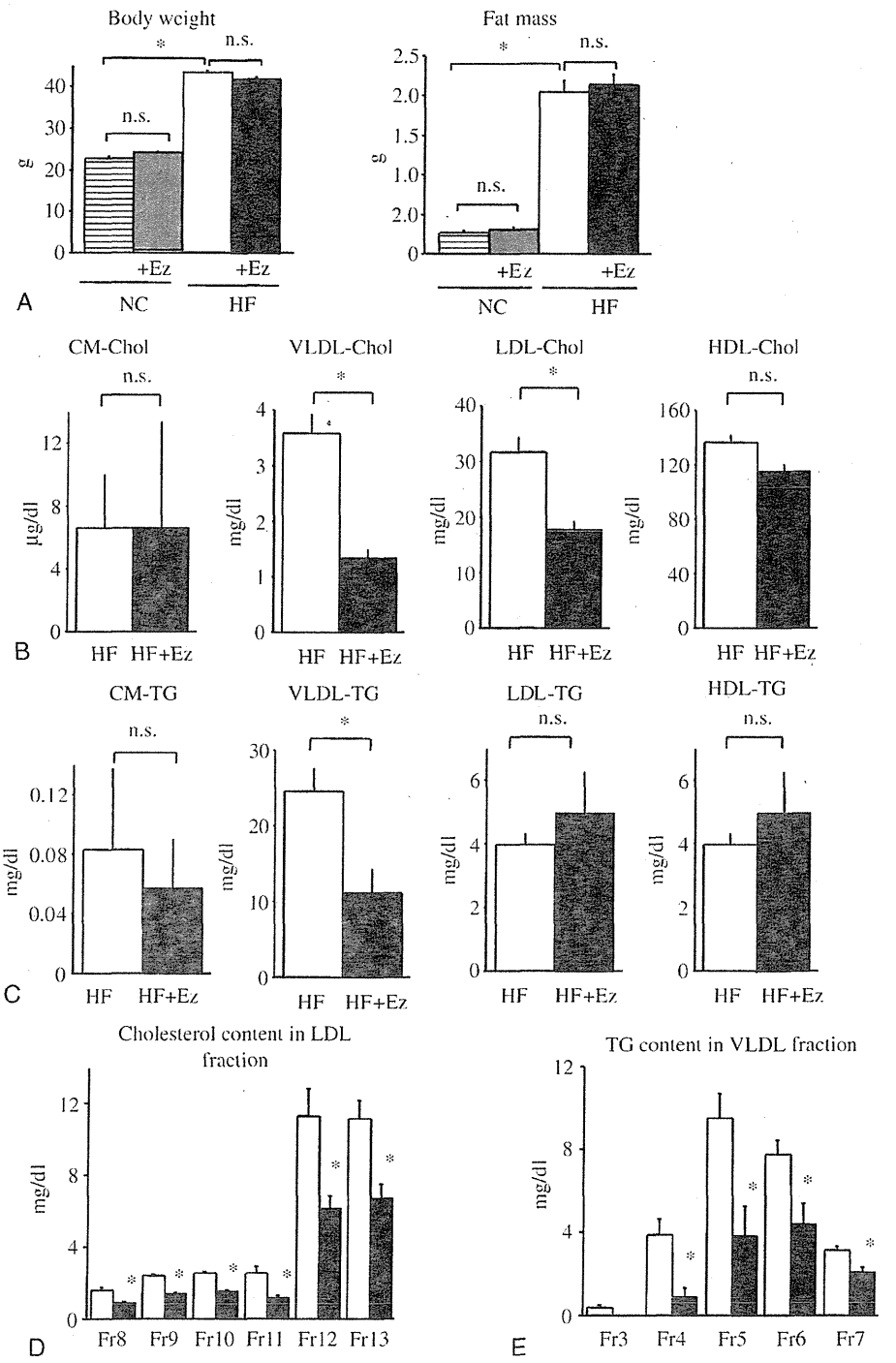

Fig. 1. Impact of ezetimibe on body weight, fat mass, and lipid metabolism in mice fed either a normal chow diet or a high-fat diet. A, Body weight and epididymal fat weight after 12 weeks on either diet. Mice were fed NC (striped bar), NC + Ez (gray bar), HF (open bar), or HF + Ez (filled bar) (n = 9-13). B, Cholesterol content in each lipoprotein in the HF (open bar) and HF + Ez (filled bar) groups (n = 6). The cholesterol contents in chylomicron, VLDL, LDL, and high-density lipoprotein were determined. C, Triglyceride content in each lipoprotein in the HF and HF + Ez groups (n = 6). The TG contents in chylomicron, VLDL, LDL, and high-density lipoprotein were determined. D, Cholesterol content in LDL fraction further analyzed in 6 subfractions according to particle size (n = 6). E, Triglyceride content in VLDL further analyzed in 6 subfractions according to particle size (n = 6). Values are the means ± SE. $^*P < .05$. CM indicates chylomicron; HDL, high-density lipoprotein.

high-fat chow or high-fat chow containing 0.005% wt/wt ezetimibe for 2 weeks. Body weight, fat mass, liver weight, and fasting plasma glucose were measured at the indicated time points after injection; and total RNA was prepared. Insulin tolerance test was conducted at the indicated time point: Mice were given free access to food and were then intraperitoneally injected with 1.5 mU of insulin per gram of body weight.

2.13. Statistical analysis

Results were expressed as the means ± SEM. Statistical differences were analyzed using the Student *t* test for unpaired comparisons and Scheffe test for comparisons among the 3 or 4 groups of mice using StatView software, version 5.0 (SAS, Cary, NC). A P value < .05 was considered statistically significant.

3. Results

3.1. No impact of ezetimibe on body weight or fat mass in mice fed a normal chow or high-fat diet

A high-fat diet treatment significantly increased body weight and fat mass, but the 2-week administration of

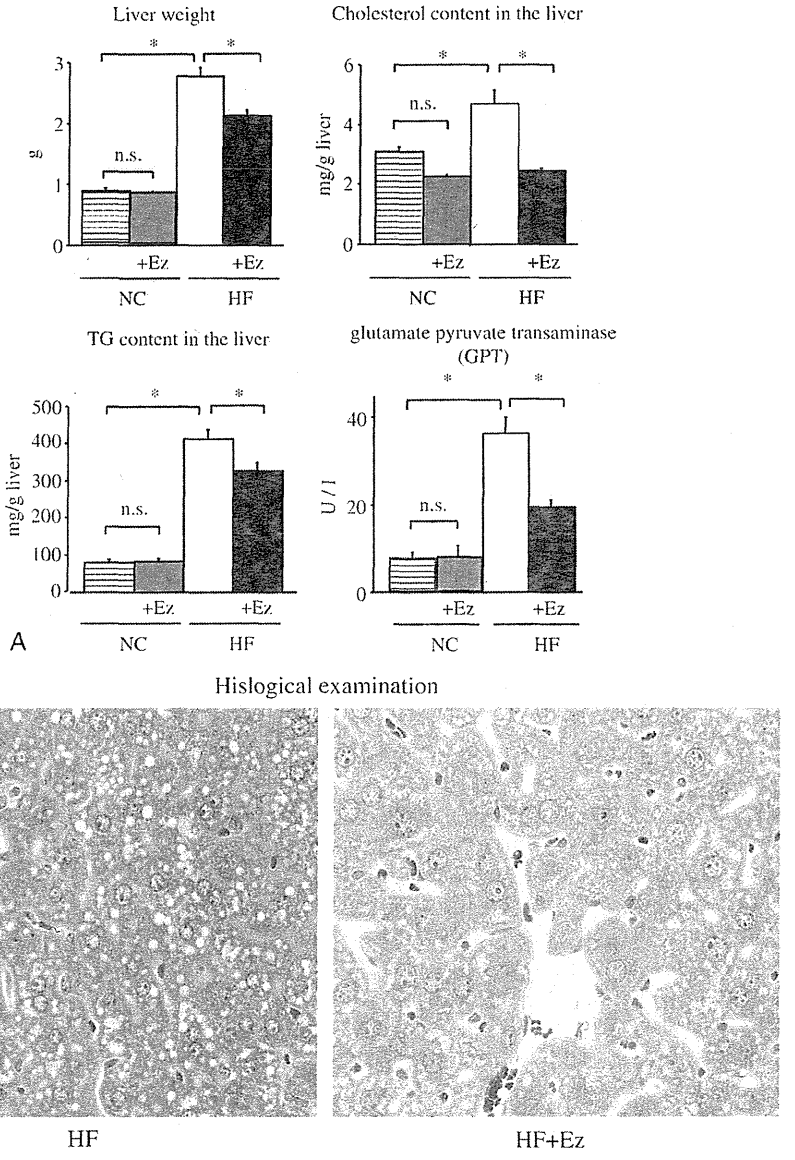

Fig. 2. Impact of ezetimibe on liver steatosis in mice fed a normal chow diet or a high-fat diet. A, Liver weights in the NC, NC + Ez, HF, and HF + Ez groups (n = 9-13). The TG contents (n = 9-10) and cholesterol contents (n = 5) in the livers of the NC, NC + Ez, HF, and HF + Ez groups are shown. The GPT levels in the NC, NC + Ez, HF, and HF + Ez groups are also shown (n = 9-13). B, Histologic analysis of liver samples stained with hematoxylin and eosin (100×) in the HF and HF + Ez groups. The values are the means ± SE. *P < .05.

ezetimibe had no impact on body weight or fat mass in mice fed either a high-fat diet or a normal chow diet (Fig. 1A).

3.2. Impact of ezetimibe on lipid metabolism in mice fed a normal chow or high-fat diet

A high-fat diet significantly increased the serum LDL cholesterol level, but not the TG level (data not shown). Among animals fed a high-fat diet, the addition of ezetimibe significantly lowered the serum cholesterol in the very low-density lipoprotein (VLDL) and LDL fractions, and TG in the VLDL fraction (Fig. 1B, C). The reduction in the cholesterol content was prominent in the VLDL and LDL fractions, especially for smaller-sized particles corresponding to small dense LDL (Fig. 1D). The reduction in the TG content was also prominent in the VLDL and LDL fractions, especially for larger-sized particles corresponding to VLDL1 (Fig. 1E). By contrast, the total cholesterol, LDL cholesterol, and TG levels were unchanged between the NC and NC + Ez groups (data not shown).

3.3. Impact of ezetimibe on liver steatosis in mice fed a normal chow or high-fat diet

A high-fat diet significantly increased the liver weight, the TG content in the liver, the cholesterol content in the liver, and the glutamate pyruvate transaminase (GPT) level. Among animals fed a high-fat diet, ezetimibe significantly lowered the liver weight, the TG content in the liver, and the cholesterol content in the liver, although no significant effects on body weight or visceral fat accumulation were observed (Fig. 2A). Histologic examination revealed that ezetimibe improved high-fat-diet–induced lipid accumulation in the liver (Fig. 2B). In contrast, the liver weights, GPT levels, and hepatic TG contents were unchanged between the NC and NC + Ez groups.

3.4. Impact of ezetimibe on glucose tolerance and insulin sensitivity in mice fed a normal chow or high-fat diet

A high-fat diet significantly increased the fasting plasma glucose level. Ezetimibe had no impact on the fasting plasma glucose level of mice fed either a high-fat diet or a normal chow diet. Of note, ezetimibe significantly strengthened the hypoglycemic effect of insulin in animals fed a high-fat diet, whereas it did not affect insulin sensitivity in animals fed a normal chow diet (Fig. 3A). We next performed a glucose tolerance test. A high-fat diet exacerbated glucose tolerance, compared with a normal chow diet. Under our experimental conditions, ezetimibe had no impact on fasting and postprandial glucose levels in mice fed either a high-fat diet or a normal chow diet but reduced the serum insulin levels after glucose loading in animals fed a high-fat diet (Fig. 3B). This result was consistent with the increase in insulin sensitivity caused by ezetimibe in animals fed a high-fat diet. A hyperinsulinemic-euglycemic clamp study revealed that the administration of ezetimibe improved the GIR and EGP in the liver but did not improve peripheral insulin sensitivity (Fig. 3C). Because hyperinsulinemic-euglycemic clamp studies have been used to investigate insulin-suppressive effect on hepatic glucose production under hyperinsulinemic conditions [24], our results (Fig. 3C) suggest that ezetimibe reverses hepatic insulin resistance under hyperinsulinemic conditions rather than under basal conditions (low concentration of insulin).

To confirm the increased insulin action in mice treated with ezetimibe, we injected insulin into the inferior vena cava and examined insulin-stimulated IRS-1, IRS-2, and Akt phosphorylation. Under basal conditions (low concentration of insulin), phosphorylation of these molecules was indistinguishable between the 2 mouse groups. Ezetimibe significantly enhanced insulin-stimulated Akt phosphorylation and tended to increase insulin-stimulated IRS-2 phosphorylation, although the latter change was not significant (Fig. 3D). Thus, in animals fed a high-fat diet, ezetimibe improved hepatic insulin resistance in association with an increase in IRS-2 and Akt phosphorylation and suppressed hepatic glucose production under hyperinsulinemic conditions.

3.5. Impact of ezetimibe on changes in gene expression profiles in the livers of mice fed a high-fat diet

To identify genes that likely affect glucose and lipid metabolism, we performed a DNA microarray. Of the 45,101 genes examined, 609 were significantly overexpressed and 888 were underexpressed in the livers of the HF + Ez group compared with the livers of the HF group. Interestingly, the lower expression of SREBP-1, ACC, SCD-1, CYP7A1, and liver CPT1 and the higher expression of SREBP2, SHP, HMG-CoA synthase, HMG-CoA reductase, LDL receptor, IRS1, and STAT3 were observed in the livers of the HF + Ez group compared with the livers of the HF group (Table 2). A Taqman PCR analysis confirmed the up-regulation of SREBP-2 and SHP and the down-regulation of SREBP-1c in the livers of the HF + Ez group compared with the livers of the HF group (Fig. 4A, B). The expressions of genes involved in fatty acid β-oxidation and inflammatory reactions were mostly unaltered between the HF and HF + Ez groups, except for the expression of CPT-1 (Table 2). Expression of G6Pase was significantly decreased in the HF + Ez group compared with the HF group, but expressions of glucokinase and PEPCK were unaltered between the 2 groups (Fig. 4C).

Expression of SHP was down-regulated and that of SREBP-1c was up-regulated in the livers on the HF diet compared with those on the normal chow (Fig. 4A).

3.6. No impact of ezetimibe on insulin sensitivity in primary cultured hepatocytes

To examine the ability of ezetimibe to ameliorate hepatic insulin resistance directly in vitro, we established primary cultured hepatocytes and examined insulin-stimulated Akt phosphorylation in the presence of 25 μmol/L of ezetimibe

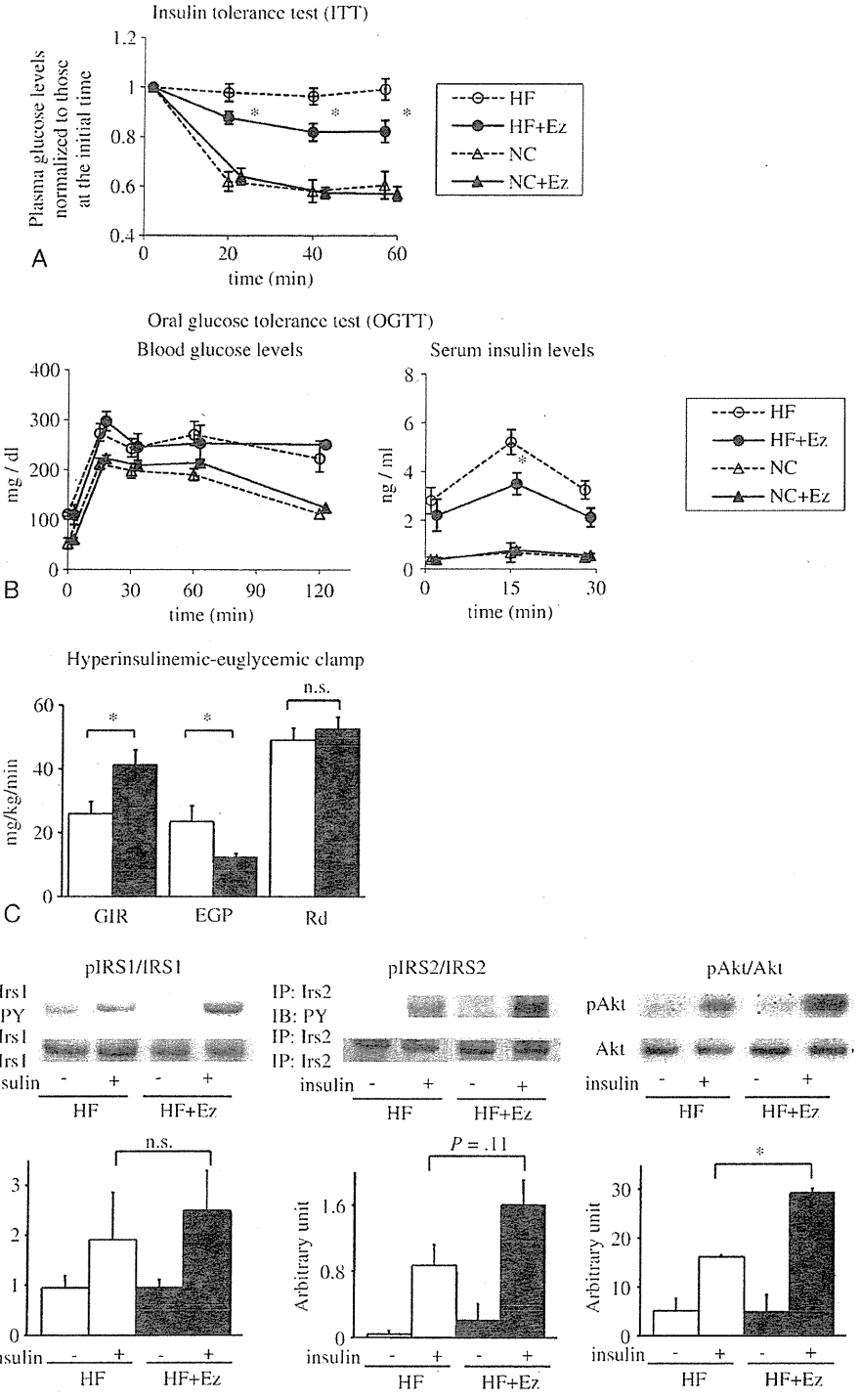

Fig. 3. Impact of ezetimibe on glucose tolerance and insulin sensitivity in mice fed a normal chow or high-fat diet. A, Blood glucose levels during insulin tolerance test in the HF (open circles), HF + Ez (filled circles), NC (open triangles), and NC + Ez (filled triangles) groups (n = 9). B, Blood glucose and plasma insulin levels during an oral glucose tolerance test conducted after 18 hours of fasting in the HF (open circles), HF + Ez (filled circles), NC (open triangles), and NC + Ez (filled triangles) groups (n = 9). C, Glucose infusion rate, EGP, and Rd in the HF (open bar) and HF + Ez (filled bar) groups in a hyperinsulinemic-euglycemic clamp study conducted after 6 hours of fasting (n = 8). D, Insulin-stimulated phosphorylation of Irs1, Irs2, and Akt in the livers of the HF (open bar) and HF + Ez (filled bar) groups (n = 4). The values are the means ± SE. *$P < .05$. HF vs HF + Ez.

Table 2
Changes in gene expression levels in the liver based on a DNA microarray analysis

SREBP pathway		
SREBP1	D	−0.5
SREBP2	I	0.9
Nuclear receptors		
SHP	I	0.5
LXRα, FXR, LRH-1	NS	
Fatty acid and TG biosynthesis		
ACC	D	−0.4
SCD-1	D	−0.5
FAS, ME	NS	
Cholesterol homeostasis and bile acid biosynthesis		
HMG-CoA synthase	I	0.4
HMG-CoA reductase	I	1.4
LDL receptor	I	0.4
CYP7A1	D	−0.9
CYP8B1, ABCA, ABCG5	NS	
Fatty acid β-oxidation		
CPT-1	D	−0.9
MCAD, LCAD	NS	
Insulin signaling		
IRS1	I	0.3
STAT3	I	−1.0
IRS2, CREB, TORC2, CBP, FOXO1, PGC1α	NS	
Inflammatory reactions		
NF-κB, JNK, TNF-α, IKKB, MCP-1, MIP-1α, IL-6	NS	

Log ratios are based on comparisons of HF + Ez vs HF. I indicates increase; D, decrease; NS, no significant change.

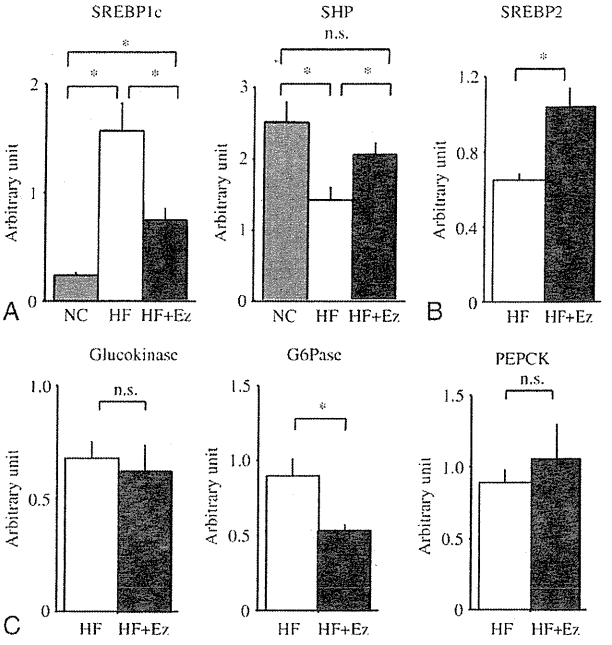

Fig. 4. Impact of ezetimibe on changes in gene expression profiles in the liver. A, Results of Taqman PCR analyses of the expression levels of SREBP-c and SHP in the livers of the NC (gray bar), HF (open bar), and HF + Ez (filled bar) groups (n = 4-6). B, Results of Taqman PCR analyses of the expression levels of SREBP2 in the livers of the HF (open bar) and HF + Ez (filled bar) groups (n = 6). The values are the means ± SE. *$P < .05$. C, Results of Taqman PCR analyses of the expression levels of Gck, G6Pase, and PEPCK in the livers of the HF (open bar) and HF + Ez (filled bar) groups (n = 8-9). The values are the means ± SE. *$P < .05$.

or dimethyl sulfoxide, followed by treatment with 10 nmol/L of insulin. Ezetimibe did not enhance insulin-stimulated Akt phosphorylation in murine cells (Fig. 5), indicating that the improvement in insulin sensitivity induced by ezetimibe in vivo (Fig. 3C, D) cannot be explained by a direct effect on the liver.

3.7. Total bile acid in the serum and liver

The total bile acid concentrations in the serum were very low and indistinguishable among the 4 groups (Fig. 6A). A high-fat diet treatment drastically decreased the total bile acid content in the liver, and ezetimibe significantly increased the total bile acid content in the livers of animals fed a high-fat diet (Fig. 6B).

3.8. RNA interference targeting SHP

To examine the role of SHP in hepatic insulin sensitivity, we performed RNA interference targeting SHP (SHP siRNA). Intravenous injection of siRNA silenced gene expression posttranscriptionally mainly in the liver [25-27] (Fig. 7A). SHP siRNA reduced SHP messenger RNA levels in the liver 24 hours after an injection, but the effects diminished by day 14. SHP siRNA did not significantly affect SREBP-1c expression in the liver under fasting conditions. At day 14, SHP siRNA significantly exacerbated the hypoglycemic effect of insulin in animals fed a high-fat diet (Fig. 7B), whereas it did not affect body weight, fat mass, or liver weight (Fig. 7C). Meanwhile, ezetimibe protected against SHP siRNA-mediated worsening of insulin resistance (Fig. 7B). These results suggest that SHP silencing mainly in the liver worsened insulin resistance and ezetimibe

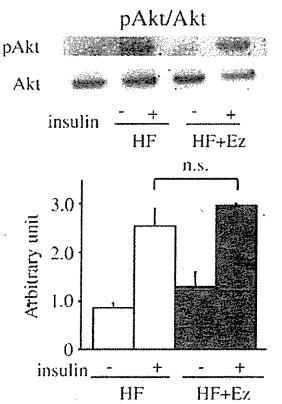

Fig. 5. No impact of ezetimibe on insulin sensitivity in primary cultured hepatocytes. The hepatocytes were incubated with or without ezetimibe (25 μmol/L) for 48 hours, followed by stimulation with insulin (10 nmol/L) for 5 minutes. An immunoblotting analysis was then performed (n = 3). The values are the means ± SE. *$P < .05$.

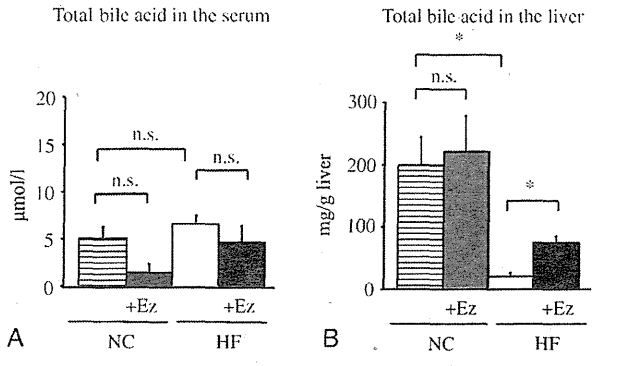

Fig. 6. Total bile acid in the serum and liver. A, Total bile acid levels in the NC, NC + Ez, HF, and HF + Ez groups (n = 5). B, Total bile acid content in the liver of the NC, NC + Ez, HF, and HF + Ez groups (n = 8). The values are the means ± SE. *$P < .05$.

protected mice from insulin resistance associated with the reduction of SHP.

4. Discussion

Previous studies have revealed a potential effect of ezetimibe on insulin sensitivity and glucose metabolism [4,10], but the mechanism responsible for the reversal of insulin resistance has remained unclear. Here, we attempted to reveal the mechanism to explain the effect of ezetimibe on insulin sensitivity and glucose metabolism using C57BL/6 mice with high-fat-diet–induced obesity. We here report 6 findings that link ezetimibe to the reversal of hepatic insulin resistance. First, a euglycemic-hyperinsulinemic clamp study revealed that ezetimibe improved the GIR and EGP in the liver but did not improve peripheral insulin sensitivity (Fig. 3C). Second, ezetimibe improved insulin signaling in the liver, as evidenced by an increase in Akt phosphorylation and a tendency to increase IRS-2 phosphorylation in animals fed a high-fat diet (Fig. 3D). Third, ezetimibe up-regulated SREBP-2 and SHP expression and down-regulated SREBP-1c expression in the liver (Fig. 4). Consistent with these alterations, fatty acid and TG synthesis was suppressed, despite the up-regulation of cholesterol synthesis (Table 2). Fourth, ezetimibe had no impact on insulin sensitivity in primary cultured hepatocytes (Fig. 5). Fifth, a high-fat diet decreased the total bile acid content in the liver; and ezetimibe partially increased it (Fig. 6B). Sixth, SHP silencing mainly in the liver worsened insulin resistance; and ezetimibe protected mice from insulin resistance associated with the reduction of SHP (Fig. 7B). These findings led to our presumption that ezetimibe reverses hepatic insulin resistance via a pathway involving SHP and SREBP-1c in animals fed a high-fat diet.

Unlike rat and human NPC1L1 protein, which is abundantly expressed in the liver, mouse NPC1L1 is predominantly expressed in the intestine [1]. Although it was reported that ezetimibe directly enhanced insulin signaling in HepG2 cells [4], the mechanism seems unlikely to be responsible for the effect of ezetimibe in mice. Thus, NPC1L1 is hardly expressed in murine liver [1]. Consistent with this assumption, ezetimibe had no impact on insulin sensitivity in primary cultured murine hepatocytes (Fig. 5).

Ezetimibe improved insulin signaling in the liver, as evidenced by the increase in Akt phosphorylation, the up-regulation of SHP expression, and the down-regulation of SREBP-1c expressions. What is the molecular link between the up-regulation of SHP, the down-regulation of SREBP-1c, and the reversal of hepatic insulin resistance? The central role of SHP in the process of inhibiting the LXR-SREBP-1c cascade has been reported in studies using SHP knockout mice and pharmacologic experiments [28]. SREBP-1c directly represses the transcription of IRS-2 and inhibits hepatic insulin signaling by inhibiting the downstream PI3K/Akt pathway, leading to a reduction in glycogen synthesis [29]. On the other hand, Yamagata et al [30] reported that bile acids suppress hepatic glucose production in an SHP-dependent fashion, suggesting a potential effect of SHP in the amelioration of insulin resistance via a non–SREBP-1c pathway. This result is consistent with our result that SHP siRNA did not affect SREBP-1c expression in the liver under fasting conditions. However, because expression of SREBP-1c under refed conditions is extremely different from that under fasting conditions [31], further studies are needed to determine whether SHP lowing worsens insulin resistance via SREBP-1c or non–SREBP-1c pathway. Nevertheless, these studies [28-30] support our presumption that ezetimibe reverses hepatic insulin resistance via a pathway involving SHP and SREBP-1c in animals fed a high-fat diet. Furthermore, the presumption is consistent with our result that SHP silencing mainly in the liver worsened insulin resistance and ezetimibe protected mice from SHP-lowing–mediated insulin resistance (Fig. 7B).

It should also be noted that expression of SHP was down-regulated and SREBP-1c was highly up-regulated in the livers of mice fed a high-fat diet compared with the livers of mice fed a normal chow diet. This fact could be one explanation why ezetimibe had no impact on insulin sensitivity in mice fed a normal chow diet, although it reversed hepatic insulin resistance in mice fed a high-fat diet. To sum up, ezetimibe may down-regulate SREBP-1c by up-regulating SHP in the liver and reverses hepatic insulin resistance in mice that have highly expressed SREBP-1c level in the liver.

What is the mechanism for the ezetimibe-induced up-regulation of SHP? SHP is induced in a bile acid–dependent manner in the presence of FXR [32,33] and functions as a direct regulator, consistent with a negative feedback loop in which increased bile acid levels result in a compensatory decrease in the rate of bile acid synthesis [34]. In fact, Watanabe et al [28] demonstrated that bile acids prevent hepatic TG accumulation and VLDL secretion via a pathway involving the up-regulation of SHP and the down-regulation of SREBP-1c in mice fed a high-fat diet. They suggested that

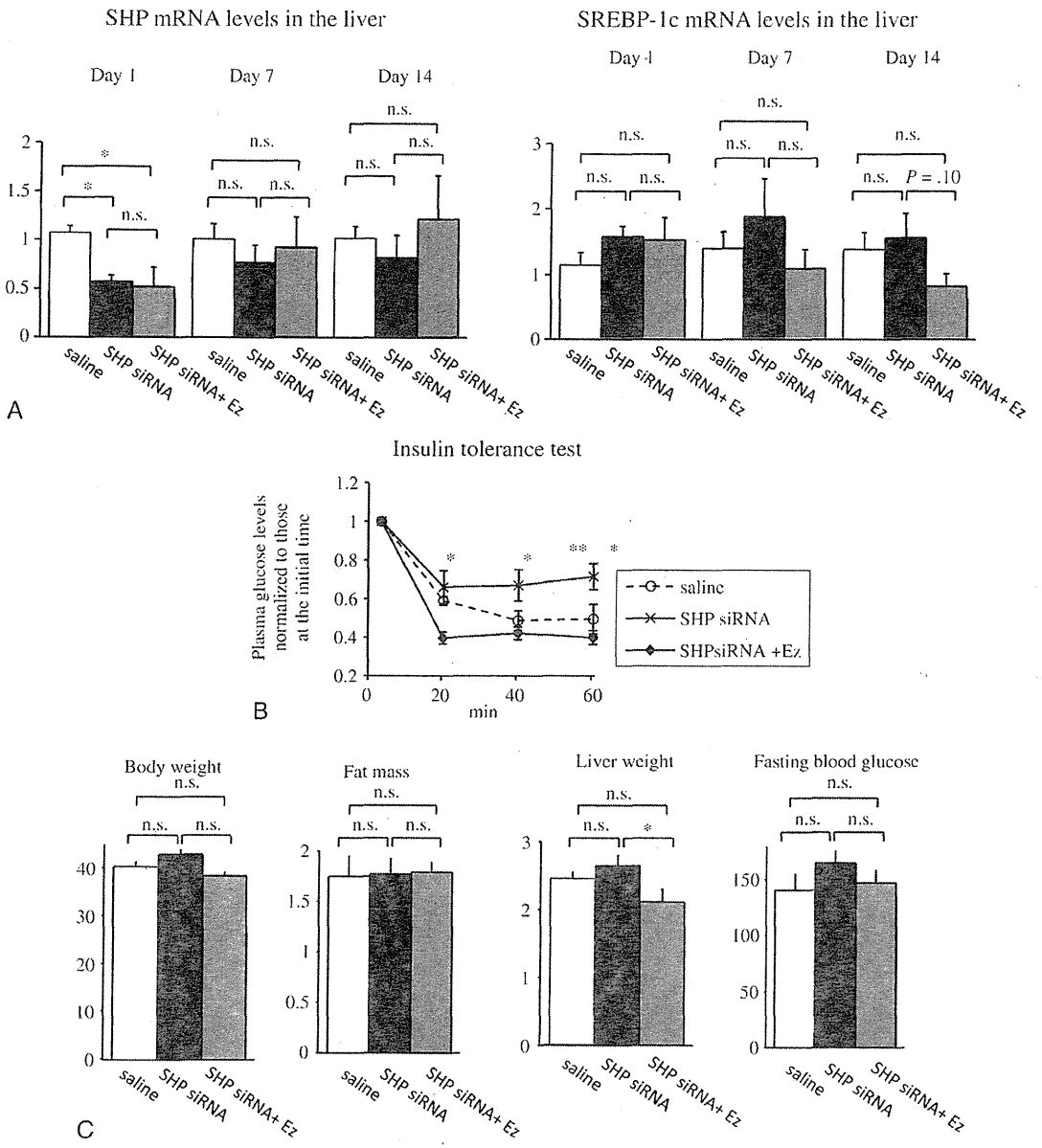

Fig. 7. Impact of intravenous injection of SHP siRNA on body weight, fat mass, liver weight, fasting blood glucose, and insulin sensitivity in mice fed a high-fat diet. A, Results of Taqman PCR analyses of the expression levels of SHP and SREBP-1c in the livers obtained from mice that were injected with saline (open bar), injected with SHP siRNA (filled bar), or treated with ezetimibe after injection of SHP siRNA (gray bar) (n = 3-4). B, Blood glucose levels during insulin tolerance test in mice fed a high-fat diet that were injected with saline (open circle), injected with SHP siRNA (asterisk), or treated with ezetimibe after injection of SHP siRNA (filled square) (n = 4-5). The values are the means ± SE. $*P < .05$ compared with SHP siRNA + Ez. $**P < .05$ compared with saline. C, Body weight, fat mass, liver weight, and fasting blood glucose of mice fed a high-fat diet that were injected with saline (open bar), injected with SHP siRNA (filled bar), or treated with ezetimibe after injection of SHP siRNA (gray bar) (n = 4-5). The values are the means ± SE. $*P < .05$.

a diet-induced increase in the bile acid content in the liver might lead to the up-regulation of SHP. Importantly, ezetimibe increased the total bile acid content in the liver in vivo, despite the down-regulation of CYP7A1 and the absence of any changes in the expressions of CYP8B1, LRH-1, ABCA, or ABCG5 (Table 2). These results suggest that the increased total bile acid content in liver cannot be explained by either an increase in bile acid synthesis or a decrease in the secretion of bile acid in the bile. In fact, it was reported that ezetimibe had no effect on bile acid synthesis in humans or in animal models [3,35,36]. Because the primary effect of ezetimibe is the inhibition of NPC1L1-mediated cholesterol absorption in the intestine, ezetimibe may up-regulate a compensatory uptake of micelle components containing cholesterol, a process that is bile acid dependent but NPC1L1 independent [1,33]. Further research is required

to elucidate how ezetimibe appears to increase the total bile acid content in the liver of C57BL/6 mice fed the types of diets used in the present studies.

What is the relevance of our results to clinical practice in human subjects with insulin resistance? The results of our study indicate that ezetimibe might be effective for ameliorating hepatic insulin resistance under hyperinsulinemic conditions. By contrast, ezetimibe had no substantial impact on insulin sensitivity in animals fed a normal chow diet. This fact suggests that the effectiveness of ezetimibe on improving hepatic insulin sensitivity is dependent on the expression level of SREBP-1c in the liver. Ezetimibe lowered the serum LDL cholesterol level in mice fed a high-fat diet, but failed in mice fed a normal chow diet. The cholesterol content in the normal chow diet was larger than in the high-fat diet (Table 1), but cholesterol absorption can also be affected by body weight and serum cholesterol level itself [37,38]. We therefore assume that high-fat-diet–induced obesity and hypercholesterolemia markedly increased cholesterol absorption in mice fed a high-fat diet and that ezetimibe was more effective under such conditions.

In conclusion, the results of our study support the concept that ezetimibe may ameliorate hepatic insulin resistance as well as dyslipidemia and hepatic steatosis via a pathway involving SHP and SREBP-1c in high-fat-diet–induced obese mice.

Acknowledgment

We are grateful to the Schering-Plough Research Institute for providing us with the ezetimibe used in this study. We thank Mitsuyo Kaji and Eri Sakamoto for their excellent technical assistance and animal care. This work was supported by the Yokohama City University Center of Excellence Program of MEXT and a grant for the Strategic Research Project of Yokohama City University (to YT).

References

[1] Altmann SW, Davis HR, Zhu LJ, Yao X, Hoos LM, Tetzloff G, et al. Niemann-Pick C1 Like 1 protein is critical for intestinal cholesterol absorption. Science 2004;303:1201-4.

[2] Davies JP, Scott C, Oishi K, Liapis A, Ioannou YA. Inactivation of NPC1L1 causes multiple lipid transport defects and protects against diet-induced hypercholesterolemia. J Biol Chem 2005;280:12710-20.

[3] Valasek MA, Repa JJ, Quan G, Dietschy JM, Turley SD. Inhibiting intestinal NPC1L1 activity prevents diet-induced increase in biliary cholesterol in Golden Syrian hamsters. Am J Physiol Gastrointest Liver Physiol 2008;295:813-22.

[4] Deushi M, Nomura M, Kawakami A, Haraguchi M, Ito M, Okazaki M, et al. Ezetimibe improves liver steatosis and insulin resistance in obese rat model of metabolic syndrome. FEBS Lett 2007;581:5664-70.

[5] Labonté ED, Camarota LM, Rojas JC, Jandacek RJ, Gilham DE, Davies JP, et al. Reduced absorption of saturated fatty acids and resistance to diet-induced obesity and diabetes by ezetimibe-treated and Npc1l1−/− mice. Am J Physiol Gastrointest Liver Physiol 2008; 295:776-83.

[6] Assy N, Grozovski M, Bersudsky I, Szvalb S, Hussein O. Effect of insulin-sensitizing agents in combination with ezetimibe, and valsartan in rats with non-alcoholic fatty liver disease. World J Gastroenterol 2006;12:4369-76.

[7] Zheng S, Hoos L, Cook J, Tetzloff G, Davis Jr H, van Heek M, et al. Ezetimibe improves high fat and cholesterol diet-induced non-alcoholic fatty liver disease in mice. Eur J Pharmacol 2008;584: 118-24.

[8] Knopp RH, Dujovne CA, Beaut AL, Lipka LJ, Suresh R, Veltri EP. Evaluation of the efficacy, safety, and tolerability of ezetimibe in primary hypercholesterolaemia: a pooled analysis from two controlled phase III clinical studies. Int J Clin Pract 2003;57:363-8.

[9] Browning JD, Horton JD. Molecular mediators of hepatic steatosis and liver injury. J Clin Invest 2004;114:147-52.

[10] González-Ortiz M, Martínez-Abundis E, Kam-Ramos AM, Hernández-Salazar E, Ramos-Zavala MG. Effect of ezetimibe on insulin sensitivity and lipid profile in obese and dyslipidaemic patients. Cardiovasc Drug Ther 2006;20:143-6.

[11] Davis Jr HR, Compton DS, Hoos L, Tetzloff G. Ezetimibe, a potent cholesterol absorption inhibitor, inhibits the development of atherosclerosis in ApoE knockout mice. Arterioscler Thromb Vasc Biol 2001;21:2032-8.

[12] Folch J, Lees M, Sloane Stanley GH. A simple method for the isolation and purification of total lipids from animal tissues. J Biol Chem 1957;226:497.

[13] Usui S, Hara Y, Hosaki S, Okazaki M. A new on-line dual enzymatic method for simultaneous quantification of cholesterol and triglycerides in lipoproteins by HPLC. J Lipid Res 2002;43:805-14.

[14] Udagawa H, Kitaoka C, Sakamoto T, Kobayashi-Hattori K, Oishi Y, Arai S, et al. Serum cholesterol–decreasing effect of heat-moisture–treated high-amylose cornstarch in cholesterol-loaded rats. Biosci Biotechnol Biochem 2008;72:880-4.

[15] Terauchi Y, Takamoto I, Kubota N, Matsui J, Suzuki R, Komeda K, et al. Glucokinase and IRS-2 are required for compensatory beta cell hyperplasia in response to high-fat diet–induced insulin resistance. J Clin Invest 2007;117:246-57.

[16] Aoki K, Matsui J, Kubota N, Nakajima H, Iwamoto K, Takamoto I, et al. The role of the liver in glucose homeostasis in PI 3-kinase p85α deficient mice. Am J Physiol Endocrinol Metab 2009;296:E842-53.

[17] Kubota N, Terauchi Y, Kubota T, Kumagai H, Itoh S, Satoh H, et al. Pioglitazone ameliorates insulin resistance and diabetes by both adiponectin-dependent and -independent pathways. J Biol Chem 2006;281:8748-55.

[18] Suzuki R, Tobe K, Aoyama M, Inoue A, Sakamoto K, Yamauchi T, et al. Both insulin signaling defects in the liver and obesity contribute to insulin resistance and cause diabetes in Irs2(−/−) mice. J Biol Chem 2004;279:25039-49.

[19] Kubota N, Terauchi Y, Tobe K, Yano W, Suzuki R, Ueki K, Takamoto I, et al. Insulin receptor substrate 2 plays a crucial role in beta cells and the hypothalamus. J Clin Invest 2004;114:917-27.

[20] Berry MN, Friend DS. High-yield preparation of isolated rat liver parenchymal cells: a biochemical and fine structural study. J Cell Biol 1969;43:506-20.

[21] Seglen PO. Incorporation of radioactive amino acids into protein in isolated rat hepatocytes. Biochim Biophys Acta 1976;442:391-404.

[22] Shiroyama K, Moriwaki K, Yuge O. The direct effect of dopamine on glucose release from primary cultured rat hepatocytes. In Vivo 1998;12:527-9.

[23] Zhang G, Budker V, Wolff JA. High levels of foreign gene expression in hepatocytes after tail vein injections of naked plasmid DNA. Hum Gene Ther 1999;10:1735-7.

[24] Bisbis S, Bailbe D, Tormo MA, Picarel-Blanchot F, Derouet M, Simon J, et al. Insulin resistance in the GK rat: decreased receptor number but normal kinase activity in liver. Am J Physiol 1993;265:807-13.

[25] Song E, Lee SK, Wang J, Ince N, Ouyang N, Min J, et al. RNA interference targeting Fas protects mice from fulminant hepatitis. Nat Med 2003;9:226-7.

[26] McCaffrey AP, Meuse L, Pham TT, Conklin DS, Hannon GJ, Kay MA. RNA interference in adult mice. Nature 2002;418:38-9.

[27] Lewis DL, Hagstrom JE, Loomis AG, Wolff JA, Herweijer H. Efficient delivery of siRNA for inhibition of gene expression in postnatal mice. Nat Genet 2002;32:107-8.
[28] Watanabe M, Houten SM, Wang L, Moschetta A, Mangelsdorf DJ, Heyman RA, et al. Bile acids lower triglyceride levels via a pathway involving FXR, SHP, and SREBP-1c. J Clin Invest 2004;113: 1408-18.
[29] Ide T, Shimano H, Yahagi N, Matsuzaka T, Nakakuki M, Yamamoto T, et al. SREBPs suppress IRS-2–mediated insulin signalling in the liver. Nat Cell Biol 2004;6:351-7.
[30] Yamagata K, Daitoku H, Shimamoto Y, Matsuzaki H, Hirota K, Ishida J, et al. Bile acids regulate gluconeogenic gene expression via small heterodimer partner-mediated repression of hepatocyte nuclear factor 4 and Foxo1. J Biol Chem 2004;279:23158-65.
[31] Kamei Y, Miura S, Suganami T, Akaike F, Kanai S, et al. Regulation of SREBP1c gene expression in skeletal muscle: role of retinoid X receptor/liver X receptor and forkhead-O1 transcription factor. Endocrinology 2008;149:2293-305.
[32] Goodwin B, Jones SA, Price RR, Watson MA, McKee DD, Moore LB, et al. A regulatory cascade of the nuclear receptors FXR, SHP-1, and LRH-1 represses bile acid biosynthesis. Mol Cell 2000; 6:517-26.
[33] Lu TT, Makishima M, Repa JJ, Schoonjans K, Kerr TA, Auwerx J, et al. Molecular basis for feedback regulation of bile acid synthesis by nuclear receptors. Mol Cell 2000;6:507-15.
[34] Russell DW, Setchell KD. Bile acid biosynthesis. Biochemistry 1992;31:4737-49.
[35] Repa JJ, Turley SD, Quan G, Dietschy JM. Delineation of molecular changes in intrahepatic cholesterol metabolism resulting from diminished cholesterol absorption. J Lipid Res 2005;46:779-89.
[36] Mathur A, Walker JJ, Al-Azzawi HH, Lu D, Swartz-Basile DA, Nakeeb A, et al. Ezetimibe ameliorates cholecystosteatosis. Surgery 2007;142:228-33.
[37] Mok HY, von Bergmann K, Grundy SM. Effects of continuous and intermittent feeding on biliary lipid outputs in man: application for measurements of intestinal absorption of cholesterol and bile acids. J Lipid Res 1979;20:389-98.
[38] Kesäniemi YA, Miettinen TA. Cholesterol absorption efficiency regulates plasma cholesterol level in the Finnish population. Eur J Clin Invest 1987;17:391-5.

GASTROENTEROLOGY 2011;140:2000–2008

BASIC—ALIMENTARY TRACT

Loss of Adiponectin Promotes Intestinal Carcinogenesis in *Min* and Wild-type Mice

MICHIHIRO MUTOH,* NAOYA TERAOKA,* SHINJI TAKASU,* MAMI TAKAHASHI,* KUNISHIGE ONUMA,* MASAFUMI YAMAMOTO,* NAOTO KUBOTA,‡ TAKAMOTO ISEKI,‡ TAKASHI KADOWAKI,‡ TAKASHI SUGIMURA,* and KEIJI WAKABAYASHI*,§

*Cancer Prevention Basic Research Project, National Cancer Center Research Institute, Tokyo, Japan; ‡Department of Diabetes and Metabolic Diseases, Graduate School of Medicine, The University of Tokyo, Tokyo, Japan; and §Graduate School of Food and Nutritional Sciences, University of Shizuoka, Shizuoka, Japan

BACKGROUND & AIMS: Metabolic syndrome- and obesity-associated cancers, including colon cancer, are common in Western countries. Visceral fat accumulation and decreased levels of plasma adiponectin (APN) have been associated with development of human colorectal adenoma. We investigated the function of APN in intestinal carcinogenesis. **METHODS:** $APN^{+/+}$, $APN^{+/-}$, or $APN^{-/-}$ mice (C57BL/6J) were given injections of azoxymethane (AOM), which led to development of intestinal tumors; these strains of mice were also crossed with *Min* mice to assess polyp formation. Adipocytokine levels and phosphorylation/activation of AMP-activated protein kinase (AMPK) were evaluated to investigate the mechanisms of APN in tumor growth. **RESULTS:** The total number of polyps in the intestines of male $APN^{+/-}$ *Min* and $APN^{-/-}$*Min* mice increased 2.4- and 3.2-fold, respectively, by the age of 9 weeks and 3.2- and 3.4-fold, respectively, by 12 weeks, compared with those of $APN^{+/+}$*Min* mice. Similar results were obtained from female mice. AOM induced colon tumor formation in 40% of $APN^{+/+}$, 50% of $APN^{+/-}$, and 71% of $APN^{-/-}$ ($P < .05$) mice, respectively; mean values for tumor multiplicity of each genotype were 0.5, 0.6, and 1.1 ($P < .05$), respectively. Phosphorylation of AMPK decreased in intestinal epithelial cells of $APN^{-/-}$ mice compared with $APN^{+/+}$ mice. Among serum adipocytokines, plasminogen activator inhibitor−1 levels increased in $APN^{-/-}$*Min* mice and $APN^{-/-}$ mice that received injections of AOM. Activation of AMPK suppressed expression of plasminogen activator inhibitor−1 in *Min* mice. **CONCLUSIONS: Mice with disruptions in *APN* develop more intestinal tumors and have decreased activation (phosphorylation) of AMPK and increased levels of plasminogen activator inhibitor−1, compared with wild-type mice. APN and its receptor might be developed as targets for cancer chemopreventive agents.**

Keywords: *Apc*-Deficient Mice; Adipokine; Colorectal Cancer; Chemoprevention

The criteria for metabolic syndrome include obesity, hyperlipidemia, type 2 diabetes, and hypertension. Several cancers, including colon cancer, are demonstrated to be associated with metabolic syndrome.[1-5] Obesity-associated cancers are common in Western countries, and they are currently increasing in Eastern countries as well. However, the mechanisms underlying how metabolic syndrome is associated with carcinogenesis remain to be fully understood. Insulin resistance, with hyperinsulinemia, hyperlipidemia, and hyperglycemia, are suggested to be involved in the promotion of colon cancer growth. In addition, dysregulation of adipocytokines, such as adiponectin (APN), leptin, plasminogen activator inhibitor-1 (PAI-1), and tumor necrosis factor−α (TNFα) has been shown to play a crucial role in the pathogenesis of the metabolic syndrome and postulated to promote carcinogenesis.[6] In human clinical studies, it has been reported that the amount of visceral fat positively correlates with colon adenoma risk, and serum APN levels show a negative correlation.[7]

APN is present at high levels in plasma (range, 3−30 μg/mL) as multimers. Both plasma APN and APN messenger RNA (mRNA) in adipose tissue are inversely correlated with body mass index and whole-body adipose mass. Furthermore, a decrease in plasma APN levels is associated with insulin resistance, type 2 diabetes, and coronary artery disease. Physiological functions of APN are elicited through 2 isoforms of its receptor, Adipo-R1 and Adipo-R2, stimulating AMP-activated protein kinase

Abbreviations used in this paper: ACF, aberrant crypt foci; AMPK, AMP-activated protein kinase; AOM, azoxymethane; APN, adiponectin; CK2β, casein kinase 2β; IL-1β, interleukin-1β; MCP-1, monocyte chemotactic protein-1; mRNA, messenger RNA; Pai-1, plasminogen activator inhibitor−1; PCR, polymerase chain reaction; RACK1, receptor for activated protein C kinase 1; TG, triglyceride; TNFα, tumor necrosis factor−α.

0016-5085/$36.00
doi:10.1053/j.gastro.2011.02.019

(AMPK) and peroxisome proliferator–activated receptor-α, respectively.[8]

Recently, we reported an age-dependent hypertriglyceridemic state with low expression levels of hepatic and intestinal lipoprotein lipase mRNA in *Apc*-deficient *Min* and *Apc*1309 mice, animal models of familial adenomatous polyposis.[9,10] Lipoprotein lipase catalyzes the hydrolysis of triglyceride (TG). Moreover, adipocytokines including plasminogen activator inhibitor–1 (Pai-1) were found to be remarkably overexpressed in the livers of *Min* mice as compared to wild-type mice.[11] In addition, hepatic APN mRNA levels were down-regulated in *Min* mice. Administration of Pai-1 blockers, SK-216 or SK-116, demonstrated the involvement of Pai-1 in the production of number of intestinal polyps.

It is assumed that adipocytokines have an impact on carcinogenesis. However, little is known about how their altered regulation is related to the development and progression of colon cancers. Thus, in the present study, we mated APN-deficient C57BL/6J mice with *Min* mice to investigate the effect of genetic inactivation of APN on intestinal carcinogenesis. APN deficiency resulted in increased intestinal polyp development. Moreover, a similar contribution was evident when APN-deficient C57BL/6J mice were treated with azoxymethane (AOM) to induce colon cancer. Reduced phosphorylated(p)-AMPK levels and increased p-Akt levels were suggested to be involved in the accelerated development of intestinal tumors. Moreover, the mechanistic consequences derived from the altered adipicytokines, APN and Pai-1, were demonstrated.

Materials and Methods

Animals

APN-deficient mice (C57BL/6J mice background) were generated as described previously and their genotypes were confirmed by polymerase chain reaction (PCR).[12] Both sexes were used at 6 weeks of age. Female C57BL/6-*Apc*$^{Min/+}$ mice (*Min* mice), 5 weeks of age, were purchased from The Jackson Laboratory (Bar Harbor, ME) and genotyped by the method reported previously. Heterozygotes of the female *Min* mice were mated with *APN*$^{-/-}$ C57BL/6J males to generate *APN*$^{+/-}$*Min* mice. Such males were crossed again with *APN*$^{+/-}$ C57BL/6J females to give *APN*$^{-/-}$*Min* mice. Offspring were genotyped by PCR.[9] In all the animal experiments in the present study, a maximum of 5 animals were housed per plastic cage, with sterilized softwood chips as bedding, in a barrier-sustained animal room, air-conditioned at 24 ± 2°C and 55% humidity, on a 12-hour light-to-dark cycle. AIN-76A powdered basal diet (CLEA Japan, Tokyo, Japan) and water were available ad libitum. The animals were observed daily for clinical signs and morbidity, and body weights and food consumption were measured weekly. At the sacrifice time point, mice were anesthetized with ether, and blood samples were collected from the abdominal vein. The experiments were conducted according to the Guidelines for Animal Experiments in the National Cancer Center and were approved by the Institutional Ethics Review Committee for Animal Experimentation in the National Cancer Center.

Experimental Protocol for APN-Deficient Min *and C57BL/6JMice*

Both sexes of *Min* mice (n = 7) with *APN*$^{+/+}$, *APN*$^{+/-}$, and *APN*$^{-/-}$ genotypes or C57BL/6J mice (n = 4) with *APN*$^{+/+}$, *APN*$^{+/-}$, and *APN*$^{-/-}$ genotypes were used for examination at the ages of 9 and 12 weeks. The levels of serum TG and total cholesterol were measured as reported previously.[10] The liver, kidneys, heart, and spleen were weighed and tissue samples from the liver and intestine were rapidly deep-frozen in liquid nitrogen and stored at −80°C.

The stomach and intestinal tract were removed, filled with 10% buffered formalin, and separated into the stomach, small intestine, cecum, and colon. The small intestine was divided into the proximal segment (4 cm in length), and proximal (middle) and distal halves of the remainder. All segments were opened longitudinally and fixed flat between filter paper in 10% buffered formalin. The numbers and sizes of polyps, and their distributions in the intestine were assessed with a stereoscopic microscope. Slices of the liver, kidneys, heart, and spleen were embedded in paraffin, sectioned, and stained with H&E.

Experimental Protocol for APN$^{+/-}$Min *Mice With APN Treatment*

Recombinant full-length murine APN was produced and purified as described previously[13,14] and dissolved in saline at a concentration of 300 μg/mL for use. *APN*$^{+/-}$*Min* mice of both sexes were divided into an APN-injected group (n = 10 each) and saline-injected control group (n = 10 each). Their body weight was measured and 1.5 mg/kg APN or the same volume of saline was intraperitoneally injected once a week from the age of 6 weeks to 12 weeks (6 times) following the method used in the previous report.[15] The numbers and sizes of polyps, and their distributions in the intestine were examined.

AOM-Induced Colon Tumor Development in APN-Deficient C57BL/6J Mice

Six-week-old male *APN*$^{+/+}$, *APN*$^{+/-}$, and *APN*$^{-/-}$ C57BL/6J mice (n = 30 each) received AOM at a dose of 10 mg/kg body weight intraperitoneally once a week for 6 weeks. Male *APN*$^{+/+}$ and *APN*$^{-/-}$ C57BL/6J mice (n = 10 each) without AOM treatment were used for evaluating sporadic colorectal cancer development. After laparotomy at 55 weeks of age, the entire intestines were resected and opened longitudinally and the contents